

# Star Cluster Formation and Evolution in Nearby Starburst Galaxies: II. Initial Conditions

R. de Grijs<sup>1\*</sup>†, P. Anders,<sup>2</sup> N. Bastian,<sup>3</sup> R. Lynds,<sup>4</sup> H.J.G.L.M. Lamers,<sup>3</sup> and E.J. O’Neil, Jr.<sup>4</sup>

<sup>1</sup> *Institute of Astronomy, University of Cambridge, Madingley Road, Cambridge CB3 0HA*

<sup>2</sup> *Universitätssternwarte, University of Göttingen, Geismarlandstr. 11, 37083 Göttingen, Germany*

<sup>3</sup> *Astronomical Institute, Utrecht University, Princetonplein 5, 3584 CC Utrecht, The Netherlands*

<sup>4</sup> *Kitt Peak National Observatory, National Optical Astronomy Observatories, Box 26732, Tucson, AZ 85726, USA*

Received date; accepted date

## ABSTRACT

We use the ages, masses and metallicities of the rich young star cluster systems in the nearby starburst galaxies NGC 3310 and NGC 6745 to derive their cluster formation histories and subsequent evolution. We further expand our analysis of the systematic uncertainties involved in the use of broad-band observations to derive these parameters (Paper I) by examining the effects of *a priori* assumptions on the individual cluster metallicities. The age (and metallicity) distributions of both the clusters in the circumnuclear ring in NGC 3310 and of those outside the ring are statistically indistinguishable, but there is a clear and significant excess of higher-mass clusters *in* the ring compared to the non-ring cluster sample; it is likely that the physical conditions in the starburst ring may be conducive for the formation of higher-mass star clusters, on average, than in the relatively more quiescent environment of the main galactic disc. For the NGC 6745 cluster system we derive a median age of  $\sim 10$  Myr. NGC 6745 contains a significant population of high-mass “super star clusters”, with masses in the range  $6.5 \lesssim \log(M_{\text{cl}}/M_{\odot}) \lesssim 8.0$ . This detection supports the scenario that such objects form preferentially in the extreme environments of interacting galaxies. The age of the cluster populations in both NGC 3310 and NGC 6745 is significantly lower than their respective characteristic cluster disruption time-scales, respectively  $\log(t_4^{\text{dis}}/\text{yr}) = 8.05$  and  $7.75$ , for  $10^4 M_{\odot}$  clusters. This allows us to obtain an independent estimate of the *initial* cluster mass function slope,  $\alpha = 2.04(\pm 0.23)_{-0.43}^{+0.13}$  for NGC 3310, and  $1.96(\pm 0.15) \pm 0.19$  for NGC 6745, respectively, for masses  $M_{\text{cl}} \gtrsim 10^5 M_{\odot}$  and  $M_{\text{cl}} \gtrsim 4 \times 10^5 M_{\odot}$ . These mass function slopes are consistent with those of other young star cluster systems in interacting and starburst galaxies.

**Key words:** galaxies: individual: NGC 3310, NGC 6745 – galaxies: starburst – galaxies: star clusters

## 1 INTRODUCTION

### 1.1 Star cluster formation in intense starbursts

The production of luminous, compact star clusters seems to be a hallmark of intense star formation. Such young clusters have been identified in intense starburst regions in several dozen galaxies, often involved in interactions (e.g., Holtzman et al. 1992, Whitmore et al. 1993, O’Connell et al.

1994, Conti et al. 1996, Watson et al. 1996, Carlson et al. 1998, de Grijs et al. 2001, 2003d). Their sizes, luminosities, and – in several cases – spectroscopic mass estimates are entirely consistent with what is expected for young Galaxy-type globular clusters (GCs; Meurer 1995, van den Bergh 1995, Ho & Filippenko 1996a,b, Schweizer & Seitzer 1998, de Grijs et al. 2001, 2003a).

It is possible, even likely, that a large fraction of the star formation in starbursts takes place in the form of such concentrated clusters (see, e.g., de Grijs et al. 2001, 2003d for a discussion). Young compact star clusters are therefore important because of what they can tell us about GC formation and evolution (e.g., destruction mechanisms and

\* E-mail: grijs@ast.cam.ac.uk

† Present address: Department of Physics & Astronomy, University of Sheffield, Hicks Building, Hounsfield Road, Sheffield S3 7RH

efficiencies). They are also important as probes of the history of star formation, chemical evolution, initial mass function (IMF), and other physical characteristics in starbursts. This is so because each cluster approximates a coeval, single-metallicity, simple stellar population (SSP). Such systems are the simplest to model, after individual stars themselves, and their ages and metallicities and – in some cases – IMFs can be estimated from their integrated spectra.

In de Grijs et al. (2003c; hereafter Paper I) we developed a reliable method to determine cluster ages, masses, metallicities and extinction values robustly and simultaneously based on imaging observations in a minimum of four broad-band passbands covering the entire optical wavelength range from the *U* to the *I* band or their equivalents in non-standard passband systems. We tested our method using the  $\sim 150$  clusters in the centre of the nearby starburst galaxy NGC 3310, and confirmed the previously suggested scenario that NGC 3310 underwent a (possibly extended) global burst of cluster formation  $\sim 3 \times 10^7$  yr ago, likely triggered by the last tidal interaction or merger with a low-metallicity, gas-rich dwarf galaxy (see Paper I).

However, in determining the cluster formation history from the age distribution of magnitude-limited cluster samples, cluster disruption must be taken into account. This is because the observed age distribution is that of the surviving clusters only. In this paper, we will therefore embark on a further analysis of the formation history of the NGC 3310 cluster system and its subsequent evolution. We will also apply our method to the star clusters and star-forming regions in the interacting galaxy NGC 6745 (the “Bird’s Head Galaxy”), and interpret its cluster formation history in the contexts of its recent tidal encounter and of cluster disruption.

## 1.2 An empirical description of cluster disruption

As shown by Boutloukos & Lamers (2003, hereafter BL03), and applied to the fossil starburst cluster sample in M82 B by de Grijs et al. (2003b), with only a few well-justified assumptions, the mass and age distributions of a magnitude-limited sample of star clusters in a given galaxy can be predicted both accurately and robustly, despite the complex physical processes underlying the assumptions (for a full discussion see BL03). If all of the following conditions are met then it can be shown easily that the age distribution of the observed cluster population will obey approximate power-law behaviours.

(i) The cluster formation rate,  $\frac{dN(M_{\text{cl}})}{dt} = S \times M_{\text{cl}}^{-\alpha}$ , is constant;

(ii) The slope  $\alpha$  of the cluster IMF is constant among cluster systems, with  $N(M_{\text{cl}})dM \propto M_{\text{cl}}^{-\alpha}dM$ ;

(iii) Stellar evolution causes SSPs to fade as  $F_{\lambda} \sim t^{-\zeta}$ , as predicted by theoretical cluster evolution models; and

(iv) The cluster disruption time depends on their initial mass as  $t_{\text{dis}} = t_4^{\text{dis}} \times (M_{\text{cl}}/10^4 M_{\odot})^{\gamma}$ , where  $t_4^{\text{dis}}$  is the disruption time-scale of a cluster with initial mass  $M_{\text{cl}} = 10^4 M_{\odot}$ .

It is well-established, however, that the disruption time-scale does not only depend on mass, but also on the initial cluster density and internal velocity dispersion (e.g., Spitzer 1957, Chernoff & Weinberg 1990, de la Fuente Marcos 1997, Portegies Zwart et al. 2001). Following the approach adopted in

BL03 and de Grijs et al. (2003b), we point out that if clusters are approximately in pressure equilibrium with their environment, we can expect the density of all clusters in a limited volume of a galaxy to be roughly similar, so that their disruption time-scale will predominantly depend on their (initial) mass (with the exception of clusters on highly-eccentric orbits). In the opposite case that the initial cluster density  $\rho$  depends on their mass  $M_{\text{cl}}$  in a power-law fashion, e.g.,  $\rho \sim M_{\text{cl}}^x$  with  $x$  being the (arbitrary) power-law exponent, the disruption time-scale will also depend on mass if  $t_{\text{dis}} \sim M_{\text{cl}}^a \rho^b$  (BL03).

The observed cluster age distribution will obey the following approximate power-law behaviours:

- $dN_{\text{cl}}/dt \propto t^{\zeta(1-\alpha)}$  for young clusters as a result of fading;
- $dN_{\text{cl}}/dt \propto t^{(1-\alpha)/\gamma}$  for old clusters as a result of disruption.

Similarly, the mass spectrum of the observed clusters will be

- $dN_{\text{cl}}/dM_{\text{cl}} \propto M_{\text{cl}}^{(1/\zeta)-\alpha}$  for low-mass clusters as a result of fading;
- $dN_{\text{cl}}/dM_{\text{cl}} \propto M_{\text{cl}}^{\gamma-\alpha}$  for high-mass clusters as a result of disruption.

Thus, both distributions will show a double power law with slopes determined by  $\alpha$ ,  $\zeta$  and  $\gamma$ . The crossing points,  $t_{\text{cross}}$  and  $M_{\text{cross}}$ , are determined by the cluster formation rate and by the  $t_4^{\text{dis}}$  time-scale. In these expressions,  $N_{\text{cl}}$  is the total number of clusters in a given sample, and so  $dN_{\text{cl}}/dM_{\text{cl}}$  and  $dN_{\text{cl}}/dt$  are the numbers of clusters per constant bin in mass and age, respectively.

In BL03 and de Grijs et al. (2003b) we showed that the observed age and mass distributions of the star cluster systems in a number of well-studied galaxies indeed show the predicted double power-law behaviour, where applicable modified by a non-constant (bursty) cluster formation rate. From the analysis of these observed distributions BL03 showed that the value of  $\gamma$  is approximately constant, ( $\gamma = 0.62 \pm 0.06$ ), under the very different environmental conditions in their sample galaxies, but the characteristic disruption time-scales (i.e.,  $t_4^{\text{dis}}$ ) differ significantly from galaxy to galaxy.

In Sect. 2 we will derive the formation history of the NGC 3310 cluster system; we will distinguish between star clusters in the starburst ring and those detected outside (Sect. 2.1), and interpret our results in the context of star cluster disruption processes and time-scales (Sect. 2.2). We will then discuss the system of young star clusters and star-forming regions in NGC 6745 in Sect. 3 in the context of its very recent tidal encounter with a small companion galaxy (Sect. 3.2), and explore the cluster properties in the framework of their disruption history (Sections 3.3 and 3.4). As we will see, both cluster systems are too young to have already undergone significant disruption, so that we are in fact observing their properties in close to initial conditions. We will discuss the derived slopes for the initial cluster mass functions for both galaxies in the general context of star cluster formation in Sect. 4, and then summarize our results and conclusions in Sect. 5.

## 2 MEASURING THE INITIAL CLUSTER MASS FUNCTION SLOPE IN NGC 3310

In Paper I we obtained robust age and mass estimates for  $\sim 150$  star clusters in the nearby starburst galaxy NGC 3310. We used a number of passband combinations based on archival *Hubble Space Telescope* (*HST*) observations from the ultraviolet (UV) to the near-infrared (NIR) to achieve this. In this paper, we will use these age and mass estimates to derive further details of the clusters' formation history and their subsequent evolution.

Figure 1a shows the distribution of the NGC 3310 clusters in the age vs. mass plane. The solid line overplotted on the figure shows the expected effect of evolutionary fading of an instantaneously formed SSP. The fading line shown is based on zero extinction, and applies to an observed cluster system with a limiting magnitude of  $V = 21$  at the distance of NGC 3310 ( $m - M = 30.57$ ; see Paper I), and our adopted, Salpeter-type IMF (with stellar masses  $m$  in the range  $0.15 \leq m/M_{\odot} \leq (50 - 70)$ , the upper limit depending on the metallicity and determined by the mass coverage of the Padova isochrones), predicted by the Göttingen SSP models (Schulz et al. 2002, updated to include nebular emission by Anders & Fritze-v. Alvensleben 2003; see also Paper I). The predicted lower limit agrees very well with our data points.

Because of the way in which we performed our cluster selection in Paper I, our adopted photometric completeness limit is ultimately determined by the interplay of two effects. These include the photometric depth of the shallowest exposure for which we required genuine source detections (i.e., the F300W image, for which we determined an average 90% completeness fraction at  $V \simeq 22$ ; see Figure 1 in Paper I) and the further loss of completeness due to the final, visual verification of the cluster candidates detected automatically. We conservatively estimate this latter step, which dominates the  $V$ -band photometry, to reduce our sample completeness by of order one more magnitude (see the detailed discussion on completeness effects for the analysis of the M51 cluster system in N. Bastian et al., in prep.), so that the limiting magnitude at  $\sim 90\%$  completeness for the full sample of NGC 3310 clusters is  $V \simeq 21$ .

For a nominal extinction of  $A_V = 0.2$  mag (see Paper I), the detection limit will shift to higher masses by  $\Delta \log(M_{cl}/M_{\odot}) \simeq 0.08$ , which is well within the uncertainties associated with our mass determinations.

Figures 1b and c show the distributions of, respectively, the ages and masses of the compact clusters in the centre of NGC 3310. The uncertainties in our fit results are of the order of the histogram bin sizes (Paper I). The open histograms, with their associated Poissonian error bars, represent the full cluster sample, whereas the shaded histograms show the effects of adopting a fixed age or mass cut-off. The shaded histogram in Fig. 1b corresponds to the clusters with masses greater than  $\log(M_{cl}/M_{\odot}) = 5.0$ , as indicated by the horizontal dotted line in Fig. 1a (arbitrarily chosen), and the shaded histogram in Fig. 1c represents (for an arbitrary age cut-off) the youngest clusters,  $\log(\text{Age}/\text{yr}) \leq 7.65$ , corresponding to the data points to the left of the vertical dotted line in Fig. 1c. The age and mass-dependent completeness limit introduces some skewness into the age and mass distributions compared to fixed age and mass cut-offs.

### 2.1 Starburst ring versus non-ring clusters

The morphology over a wide range of wavelengths (from X-rays to radio waves) of the central regions of NGC 3310 is dominated by a bright, relatively dense ring-like structure containing a large number of actively star-forming regions and young star cluster candidates (see Paper I for a review). Conselice et al. (2000) suggested a bar-driven origin for the active starburst in the ring, combined with the recent infall of a companion galaxy. Such a scenario provides a natural explanation for the low metallicity observed in the star-forming knots near the galactic centre (see Paper I for an overview), while it also explains why we observe concentrated star formation in star clusters or luminous HII regions in such a tightly-wound ring-like structure surrounding the centre (e.g., van der Kruit & de Bruyn 1976, Telesco & Gatlley 1984, Pastoriza et al. 1993, Meurer et al. 1995, Smith et al. 1996, Conselice et al. 2000, Elmegreen et al. 2002), coinciding with the end of the nuclear bar (Conselice et al. 2000, but see Díaz et al. 2000), but not inside this ring.

#### 2.1.1 A comparison of basic properties

We identified 82 of the 147 star clusters in our sample to coincide with this circumnuclear ring, with the 65 remaining objects being located *outside* this starburst ring. In Fig. 2 we compare the basic properties of these cluster samples. The peaks in the age distributions are observed at  $\log(\text{Age}/\text{yr}) = 7.45$  and  $7.43$  for the clusters in and outside the ring, respectively, with corresponding Gaussian sigmas,  $\sigma_G$ , of  $0.40$  and  $0.38$  in logarithmic age space. However, while the age (and also the metallicity) distributions of both cluster samples are statistically indistinguishable, the ring clusters appear to peak at slightly greater masses than those found outside the ring: the mass distribution of the clusters in the ring peaks at  $\log(M_{cl}/M_{\odot})_{\text{ring}} = 5.29$ , versus  $\log(M_{cl}/M_{\odot})_{\text{non-ring}} = 5.13$  for the clusters outside the ring. Their Gaussian sigmas are also significantly different, at  $\sigma_{G,\text{ring}} = 0.32$  and  $\sigma_{G,\text{non-ring}} = 0.51$ , respectively.

We examined whether this difference could be due to a spatial dependence of the completeness fraction, in the sense that one might expect a lower completeness in the ring area with its higher background flux than outside the ring. This difference in the mean (logarithmic) mass corresponds to a difference in the peak of the cluster luminosity function (CLF), in any passband, of  $\Delta m_{\text{peak}} \simeq 0.4$  mag, and the difference in the Gaussian sigmas of the distributions is also in the sense expected if this were due to different and variable levels of completeness. We examined the mean surface brightness levels in and outside the starburst ring, respectively, both in the F606W image and in the slightly shallower F300W passband. The difference in the mean surface brightness levels between the starburst ring and the area outside the ring is  $\Delta(\Sigma_{\text{non-ring}} - \Sigma_{\text{ring}}) \sim 0.3 - 0.9$  mag arcsec $^{-2}$  and  $\sim 0.1 - 0.8$  mag arcsec $^{-2}$  in the F300W and F606W images, respectively, based on a per-pixel comparison.

The overabundance of low-mass clusters outside the ring compared to their counterparts in the starburst ring might therefore (at least partially) be due to a spatial dependence of the completeness fraction. However, there is a clear and significant excess of higher-mass clusters ( $5.25 \lesssim \log(M_{cl}/M_{\odot}) \lesssim 5.75$ ) in the ring compared to the non-ring

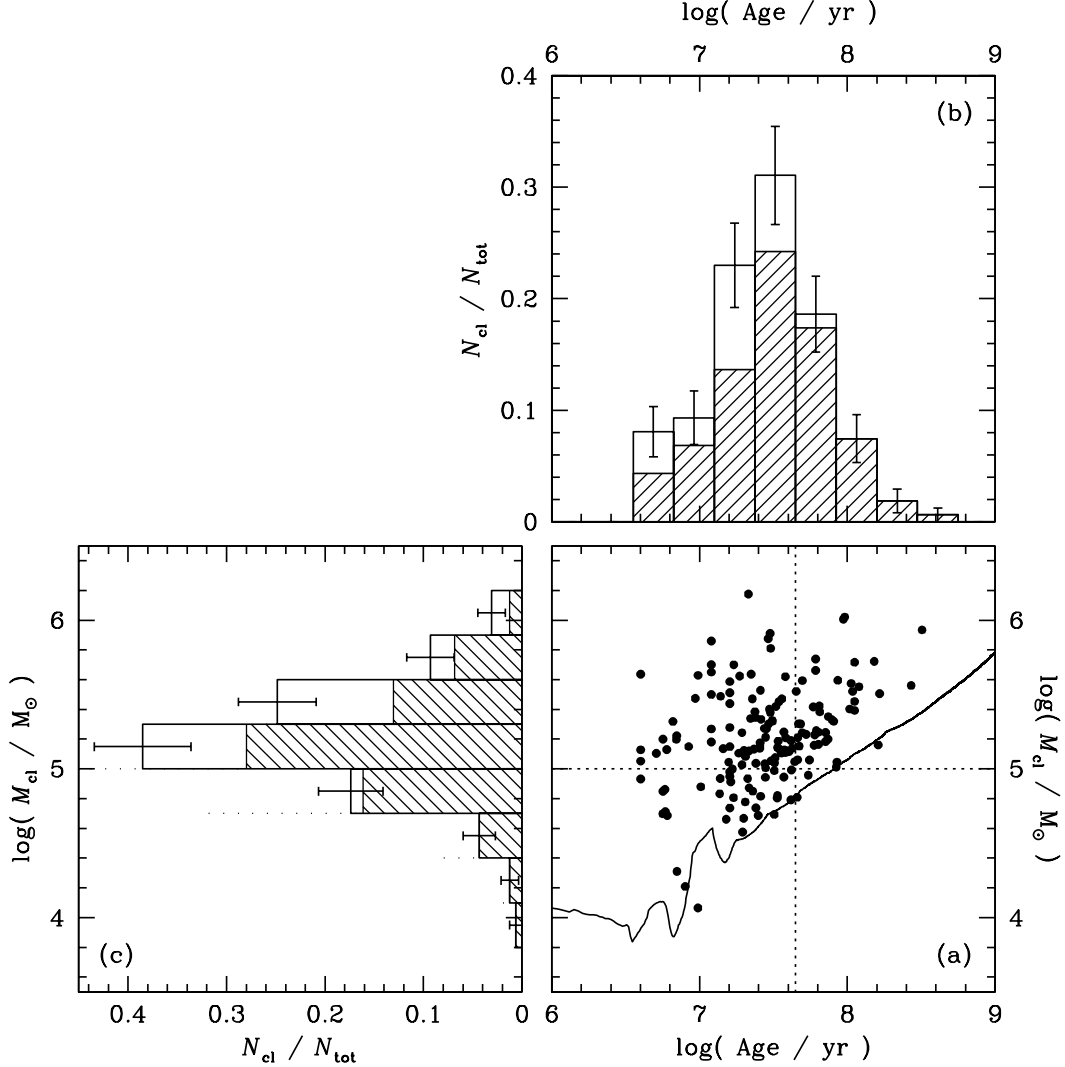


**Figure 1.** (a) – Distribution of the NGC 3310 clusters in the (age vs. mass) plane. Overplotted is the expected, age-dependent detection limit. This model prediction is based on a detection limit of  $m_{F606W} \sim V = 21$  (see text) and  $(m - M)_{\text{NGC3310}} = 30.57$ , assuming no extinction. The features around 10 Myr are caused by the appearance of red supergiants. (b) and (c) – Distributions of, respectively, the ages and masses of the compact clusters in the centre of NGC 3310. The open histograms, with their associated Poissonian error bars, represent the full cluster sample; the shaded histogram in panel (b) corresponds to the clusters with masses greater than  $\log(M_{\text{cl}}/M_{\odot}) = 5.0$ , indicated by the horizontal dotted line in panel (a), and the shaded histogram in panel (c) represents the youngest clusters,  $\log(\text{Age}/\text{yr}) \leq 7.65$ , corresponding to the data points to the left of the vertical dotted line in panel (a). The uncertainties are of the order of the histogram bin sizes.

cluster sample, even after taking the systematic uncertainties in our mass estimates into account (the estimated  $\sim 1\sigma$  systematic uncertainties are of the order of the histogram bin sizes). If both the ring and the non-ring cluster populations were drawn from the same parent population, one would not expect to observe such large differences, and thus it appears that the physical conditions in the starburst ring, such as caused by the effects of the proposed bar-driven instabilities, the higher density of the interstellar medium (ISM), and the associated higher likelihood to encounter significant propagating shock waves, may be conducive for the formation of higher-mass star clusters, on average, than in the relatively more quiescent environment of the main galactic disc. Thus, the origin of the differences in the global mass

distributions at the high-mass end of the two cluster samples is most likely found in their respective ISM properties.

If the cluster formation in the starburst ring were predominantly due to the bar-driven instabilities suggested by Conselice et al. (2000), one would, to first order, expect a narrower age distribution for the clusters in the ring with respect to that of the non-ring clusters in the general field of the central galactic disc. However, both age distributions are characterized by a median age of  $\langle \log(\text{Age}/\text{yr}) \rangle \simeq 7.5$  ( $\sim 30$  Myr), and an age spread of  $\sigma_{\text{G}}(\log[\text{Age}/\text{yr}]) \simeq 0.4$  ( $\sim 70$  Myr, from  $\sim 80 - 10$  Myr ago). Furthermore, if we examine the age distributions of the clusters in linear age space, it appears that clusters both in and outside the starburst ring have been forming approximately constantly, but

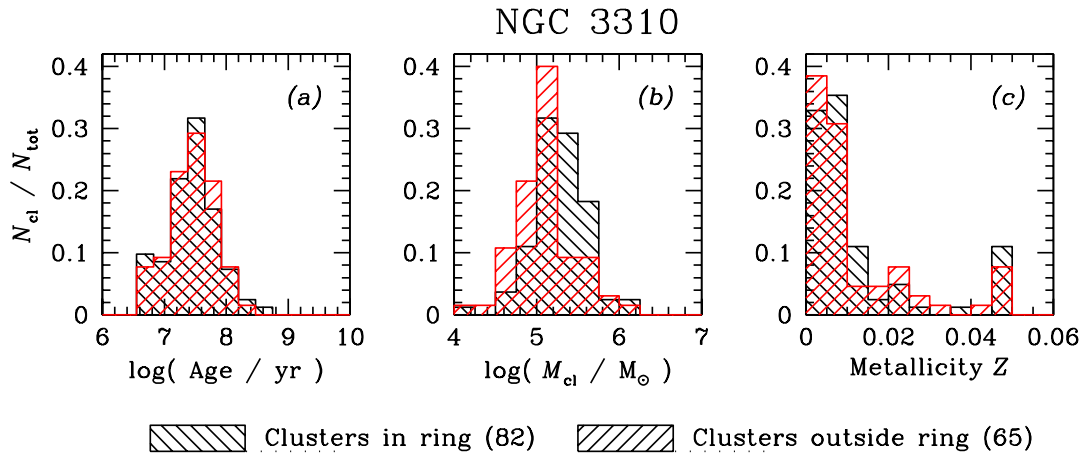


**Figure 2.** Comparison of the basic properties of the ring clusters with those of the non-ring cluster sample.

at a  $\sim 2 - 3\times$  higher level during the past  $\sim 40$  Myr than before. Thus, we conclude that the starburst producing the NGC 3310 ring clusters has been ongoing for at least the past 40 Myr, at an approximately constant cluster formation rate during the burst period. Star cluster formation has proceeded at a similar rate in the general central disc of the galaxy; due to the extreme youth of both samples of starburst-induced star clusters, statistically significant differences between the age distributions of the ring and non-ring populations have not yet had time to develop, which implies that we are still observing at least part of the cluster sample in the environment determined by their initial conditions.

### 2.1.2 Effects of metallicity changes on the systematic uncertainties

Finally, we caution that the peak of cluster formation, while relatively robust (see, e.g., Paper I for a discussion), is undoubtedly broadened by the various uncertainties entering the age-dating process. Some of these (systematic) uncertainties were discussed in detail in Paper I, where we concentrated our discussion on the choice of passband combination for this type of analysis. Here, we will try to obtain a further handle on the systematic uncertainties. If the cluster formation in the starburst ring were induced by bar-driven instabilities acting on very short time-scales (i.e., on time-scales short compared to the median age of the cluster sample), one would not expect the resulting cluster sample to be characterized by a large range in metallicity. This argument holds both if the progenitor gas clouds originated from the main NGC 3310 gas reservoir, and also if they came from a low-metallicity dwarf galaxy that was cannibalized (assuming that such a galaxy would exhibit a fairly small range in metallicities, as suggested for this particular interaction; see Paper I). The former case is further strengthened by observations in other galaxies that old galactic discs generally show smooth, very slowly declining radial metallicity gradients, such that at any given small distance range from the galactic centre (e.g., as in the NGC 3310 starburst ring) the stellar metallicity is approximately constant (for the Galaxy

see, e.g., Twarog et al. 1997, and the discussion therein). This is to some extent already reflected in Fig. 2c, where we derived that  $> 80\%$  of the clusters in the ring have metallicities  $Z < 0.015$ .

We will now assume a mean metallicity of  $Z = 0.008$  for the clusters in the starburst ring, and rederive their age and mass distributions. This will give us a further handle on the systematic, model-dependent uncertainties entering the age-dating and mass-estimation process. In Fig. 3 we show the age and mass distributions obtained under the assumption that the ring clusters all have a fixed metallicity of  $Z = 0.008$ . The peaks in the age and mass distributions occur at  $\langle \log(\text{Age}/\text{yr}) \rangle = 7.34$  and  $\langle \log(M_{\text{cl}}/M_{\odot}) \rangle = 5.09$ , respectively, while the distributions are characterized by Gaussian sigmas  $\sigma_{\text{G,age}} = 0.50$  and  $\sigma_{\text{G,mass}} = 0.42$ . As a reminder, the age and mass distributions resulting from retaining the metallicity as a free parameter (Sect. 2.1.1), were  $\langle \log(\text{Age}/\text{yr}) \rangle \simeq 7.45$  and  $\langle \log(M_{\text{cl}}/M_{\odot}) \rangle = 5.29$ , respectively, with  $\sigma_{\text{G,age}} = 0.40$  and  $\sigma_{\text{G,mass}} = 0.32$ . We see that while the peak values are retained with a reasonable robustness (although there is, as expected, some effect caused by the age–metallicity degeneracy), both distributions have broadened significantly. This confirms, therefore, that (i) it is very important to determine all of the free parameters (age, metallicity, and extinction, and the corresponding mass estimates) *independently* for each individual cluster, instead of assuming a generic value for any of these parameters (if a sufficient number of broad-band passbands covering a large wavelength range are available); and (ii) the widths of the distributions (assuming a fixed metallicity) are broader than their intrinsic widths owing to the propagation of model and measurement uncertainties (e.g., de Grijs et al. 2003b).

For comparison, we also computed the characteristics of the age and mass distributions for the NGC 3310 clusters outside the ring, under the same assumption of a fixed metallicity of  $Z = 0.008$  for all clusters. The trend between these new determinations and those of the fixed-metallicity results for the ring clusters remains similar as for the situation in which we allowed the metallicity to be an additional free parameter: the age distribution peaks again at a similar median age,  $\langle \log(\text{Age}/\text{yr}) \rangle_{\text{non-ring}} = 7.37$ , with a Gaussian

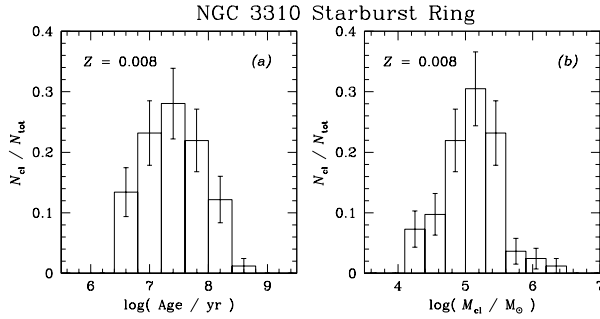


**Figure 3.** Age and mass distributions of the clusters in the NGC 3310 starburst ring, obtained under the assumption that *all* clusters have a fixed metallicity of  $Z = 0.008$ .

sigma of  $\sigma_{G, \text{non-ring}} = 0.52$ . The median of the mass distribution occurs at a significantly lower mass than for the ring clusters,  $\langle \log(M_{\text{cl}}/M_{\odot}) \rangle_{\text{non-ring}} = 4.93$ , with a Gaussian sigma of  $\sigma_{G, \text{non-ring}} = 0.60$ . Thus, we arrive at similar conclusions as before for the mass distribution of the non-ring compared to the ring sample of clusters in NGC 3310.

## 2.2 The star cluster disruption context

In Fig. 4 we show the formation rate and the mass spectrum of the entire NGC 3310 cluster sample. These distributions depend on the cluster formation history and on the cluster disruption time-scale governing the centre of NGC 3310.

For our analysis of the cluster disruption history in the centre of NGC 3310 we adopt a slope  $\zeta = 0.648$  for the evolutionary fading of clusters in the  $V$  band, derived from theoretical SSP models (see also BL03, de Grijs et al. 2003b). For the mass scaling of the disruption time-scale we adopt  $\gamma = 0.62$  (BL03, de Grijs et al. 2003b).

We also assume that the cluster formation rate has been approximately constant during the periods of interest for our analysis,  $\log(\text{Age}/\text{yr}) \lesssim 7.5$  and  $\log(\text{Age}/\text{yr}) \gtrsim 7.5$ . As shown in Sect. 2.1, this assumption seems justified, within the uncertainties.

In Fig. 4a, the long-dashed line for the youngest ages,  $\log(\text{Age}/\text{yr}) \leq 8$ , is the expected effect of a fading SSP (in the  $V$  band), for a constant ongoing cluster formation rate, shifted vertically to best match the data points for  $\log(\text{Age}/\text{yr}) \leq 7.5$ . The short-dashed lines in both Figs. 4a and b are the best-fitting power-law slopes, obtained for the age and mass ranges  $\log(\text{Age}/\text{yr}) \geq 7.7$  and  $\log(M_{\text{cl}}/M_{\odot}) \geq 5.1$ , while the dotted lines are indicative of the likely uncertainties in the slopes. The latter were obtained from subsets of the data points used for the dashed fits, determined over the full ranges. Our results are robust with respect to changes in the adopted bin size in  $\log(\text{Age}/\text{yr})$  and  $\log(M_{\text{cl}}/M_{\odot})$ . The vertical dashed line in Fig. 4b at  $\log(M_{\text{cl}}/M_{\odot}) = 4.4$  corresponds to our completeness limit, for a cluster age of  $\log(\text{Age}/\text{yr}) = 7.5$ . However, since our cluster sample is characterized by a range of ages up to  $\sim 10^8$  yr, it follows that incompleteness plays at least some role for masses up to  $\log(M_{\text{cl}}/M_{\odot}) \sim 4.9$  (see the vertical dotted line in Fig. 4b). For the age distribution the effects of incompleteness are less complicated, since they are determined solely by (the extension of) the fading line in Fig. 4a. Moreover, the effects of the non-constancy of the cluster formation rate

are less transparent and therefore harder to disentangle from the mass distribution than from the age distribution (see de Grijs et al. 2003b for a discussion).

The short-dashed line in Fig. 4a, which shows the effect of cluster disruption, has a predicted slope of  $(1 - \alpha)/\gamma$  and an observed slope of  $-2.64(\pm 0.14) \pm 0.47$ , where the first uncertainty represents the formal uncertainty in the fit and the second the likely uncertainty resulting from our choice of fitting range (i.e., the dotted fits in Figs. 4a and b). If we adopt a cluster IMF slope of  $\alpha = 2.0$  (see Sect. 4) we find that the slope of the cluster disruption law is  $\gamma \simeq 0.38 - 0.46$ , with  $t_{\text{dis}} \propto M_{\text{cl}}^{\gamma}$ . This value is smaller than the mean value of  $\gamma \simeq 0.62$  found by BL03 from cluster samples in different galaxies. The crossing point of the two power-law fits is at  $\log t_{\text{cross}} \simeq 7.7$ . Substituting this value in Eq. (15) of BL03, we find that the characteristic disruption time of a  $10^4 M_{\odot}$  cluster is  $\log t_4^{\text{dis}} = 7.9$ . This implies that the disruption time-scale of clusters with an initial mass greater than  $10^5 M_{\odot}$  will be greater than  $2 \times 10^8$  yr. The slope of the mass distribution in Fig. 4b, for clusters more massive than  $10^5 M_{\odot}$  is  $-2.04(\pm 0.23)^{+0.13}_{-0.43}$ , where the first uncertainty represents the formal uncertainty in the fit and the second the likely uncertainty resulting from our choice of fitting range. All these clusters are younger than  $2 \times 10^8$  yr. (In fact, all our sample clusters, except one, are younger than this age.) Thus, disruption has not yet affected the mass distribution of these massive clusters and hence the observed slope of the mass distribution is the slope of the cluster IMF. We note that this new value of the NGC 3310 cluster IMF slope closely matches both our earlier CLF slope determination of  $\alpha = 1.8 \pm 0.4$  obtained from the cluster mass function in Paper I, and the best estimate of Elmegreen et al. (2002),  $2.2 \lesssim \alpha \lesssim 2.4$ .

Finally, in Fig. 5 we compare the clusters in the ring with those outside the ring. Within the observational uncertainties, we do not detect any differences in the slopes of either the age or the mass distributions. This is another argument highlighting the very young age of this cluster system compared to the expected characteristic disruption time-scale, even in the higher density environment of the starburst ring.

## 3 STAR FORMATION IN THE BIRD'S HEAD GALAXY

### 3.1 Observations and data preparation

Optical observations of NGC 6745 in the minimum of four passbands spanning the entire wavelength range from the  $U$  (F336W) to the  $I$  band (F814W) were obtained between 18 and 20 March 1996, as part of *HST* GO programme 6276 (PI Westphal), using the Wide Field Planetary Camera 2 (*WFPC2*). Multiple exposures were obtained through each filter to facilitate the removal of cosmic rays; the galactic centre was placed on the WF3 chip (pixel size 0.0997 arcsec) in all cases. An overview of the available *HST* observations is given in Table 1.

Pipeline image reduction and calibration of the *WFPC2* images were done with standard procedures provided as part

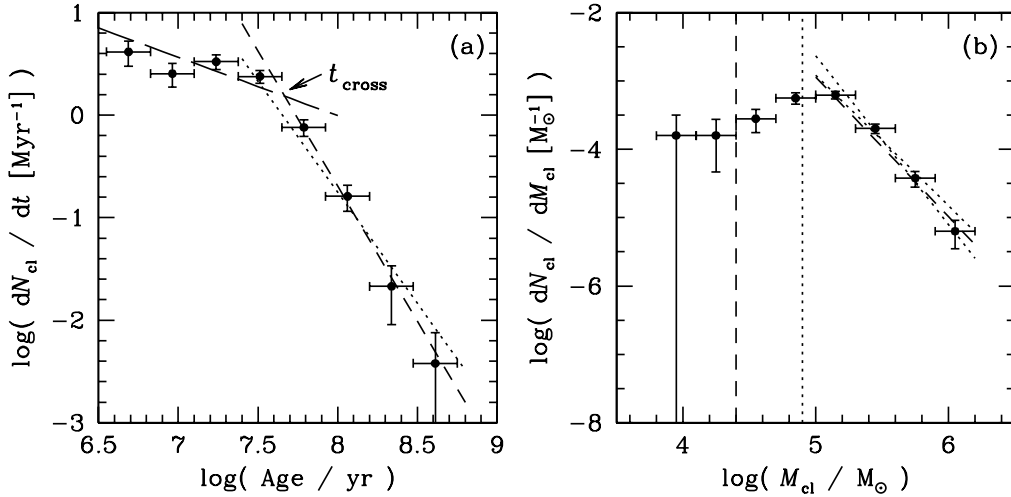


**Figure 4.** (a) – The cluster formation rate (in number of clusters per Myr) in NGC 3310 as a function of age. The long-dashed line for  $\log(\text{Age}/\text{yr}) \leq 8$  is the expected effect of a fading SSP, for a constant ongoing cluster formation rate, shifted vertically to best match the data points for  $\log(\text{Age}/\text{yr}) \leq 7.5$ . The short-dashed and dotted lines are the best-fitting and maximum deviating power-law slopes, as described in the text. (b) – Mass spectrum of the NGC 3310 clusters (number of clusters per mass bin); line encoding as in panel (a). The vertical dashed line at  $\log(M_{cl}/M_{\odot}) = 4.4$  corresponds to our completeness limit, for a cluster age of  $\log(\text{Age}/\text{yr}) = 7.5$ , while the vertical dotted line corresponds to the same completeness limit at an age of  $\log(\text{Age}/\text{yr}) = 8.0$ .

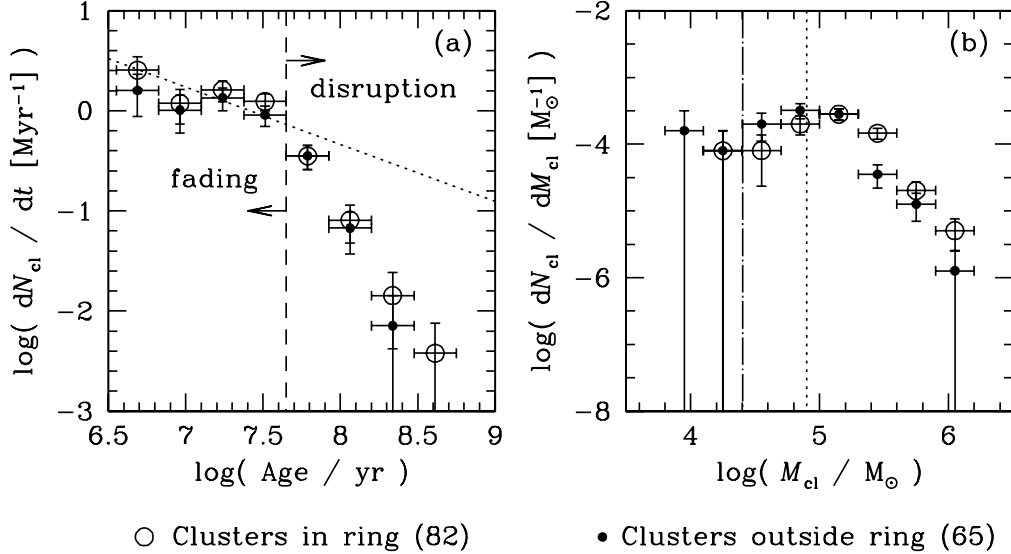


**Figure 5.** Comparison of the cluster formation rates and mass spectra of the clusters in vs. outside the NGC 3310 starburst ring. The age ranges in which stellar evolutionary fading and cluster disruption dominate are indicated; the vertical dash-dotted line in panel (b) indicates our completeness limit for a cluster age of  $\log(\text{Age}/\text{yr}) = 7.5$ , while the vertical dotted line corresponds to the same completeness limit, but at an age of  $\log(\text{Age}/\text{yr}) = 8.0$ .

of the IRAF/STSDAS<sup>‡</sup> package, using the updated and cor-

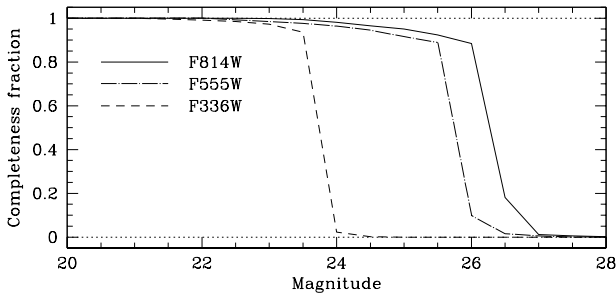
<sup>‡</sup> The Image Reduction and Analysis Facility (IRAF) is distributed by the National Optical Astronomy Observatories, which is operated by the Association of Universities for Research in Astronomy, Inc., under cooperative agreement with the National

Science Foundation. STSDAS, the Space Telescope Science Data Analysis System, contains tasks complementary to the existing IRAF tasks. We used Version 2.2 (August 2000) for the data reduction performed in this paper.

**Table 1.** Overview of the *HST* observations of NGC 6745

Filter	Exposure time (sec)	ORIENT <sup>a</sup> (°)
F336W	2400, 7×2800	145.52
F555W	2×1100	145.52
	2×1300	145.52
F675W	4×1300	145.52
F814W	4×1300	145.52

NOTE: <sup>a</sup> – Orientation of the images (taken from the image header), measured North through East with respect to the V3 axis (i.e., the X=Y diagonal of the WF3 CCD +180°).

**Figure 6.** Formal completeness curves for the full *WFPC2* field of view of the NGC 6745 observations. The different line styles refer to different passbands, as indicated in the figure.

rected on-orbit flat fields and related reference files most appropriate for the observations.

We obtained source lists and, subsequently, source photometry for all of our NGC 6745 observations following procedures identical to the ones described in detail in Paper I. For NGC 6745, at a distance  $D \simeq 68$  Mpc ( $m - M = 34.17$ ; assuming a systemic velocity  $v_{r,\odot} = 4545 \pm 60$  km s<sup>-1</sup> [Falco et al. 1999], a 208 km s<sup>-1</sup> correction for infall of the Local Group towards the Virgo cluster, and  $H_0 = 70$  km s<sup>-1</sup> Mpc<sup>-1</sup>), all compact clusters and most star forming regions appear as point-like sources. The final list of verified cluster candidates detected at at least four times the background r.m.s. noise level in all four passbands contains 177 objects.

We estimated the completeness of our source lists by using synthetic source fields consisting of PSFs. We created artificial source fields for input magnitudes between 20.0 and 28.0 mag, in steps of 0.5 mag, independently for each of the F336W, F555W, and F814W passbands. We then applied the same source detection routines used for our science images to the fields containing the combined galaxy image and the artificial sources. The results of this exercise are shown in Fig. 6. These formal completeness curves were corrected for the effects of blending or superposition of multiple randomly placed artificial PSFs as well as for the superposition of artificial PSFs on genuine objects. A detailed description of the procedures employed to obtain these completeness curves was given in Paper I.

We found that the effects of image crowding are small: only  $\lesssim 1.5$ –2.5% of the simulated objects were not retrieved due to crowding, either in the artificial or in the combined frames. However, the effects of the bright and irregular background and dust lanes are large, resulting in variable com-

pleteness fractions across the galaxy images. As a general rule, however, the curves in Fig. 6 show that the formal completeness drops below  $\sim 90\%$  for F336W  $\gtrsim 23.5$  mag, for F555W  $\gtrsim 25.5$  mag, and for F814W  $\gtrsim 26$  mag; the actual completeness limits are likely somewhat shallower, resulting from our selection criteria (cf. N. Bastian et al., in prep.).

Foreground stars are not a source of confusion. The standard Milky Way star count models (e.g., Ratnatunga & Bahcall 1985) predict roughly 1–2 foreground stars for the equivalent standard filter of F555W  $\lesssim 24$  in our field of view. Background objects may pose a (small) problem, however, in particular among the fainter sources, since we did not impose any roundness or sharpness constraints on our extended source detections, in order not to omit unrelaxed young clusters and star-forming regions from our final sample. However, such objects should be easily identifiable once we have obtained aperture photometry for our complete source lists, as they are expected to have significantly different colours. Background galaxies at redshifts greater than about 0.1 are expected to have extremely red ( $m_{F336W} - m_{F814W}$ ) colours compared to their local counterparts and the young star clusters and star forming regions expected in NGC 6745.

We will discuss the derived parameters and their implications for the evolution of the galaxy’s star cluster system in Sects. 3.3 and 3.4, respectively.

Additionally, HI 21cm observations (at  $\sim 1.399$  GHz) were obtained with all 27 antennae of the Very Large Array (VLA) in C configuration, on 28 May 2000, with an on-source exposure time of 24765 s ( $\sim 7$  hr). Primary calibrators were observed at the beginning and end; secondary (phase) calibrator integrations were uniformly interspersed throughout the run. The  $(u,v)$  plane coverage was almost perfectly isotropic, and 8192 CLEAN cycles (with uniform  $(u,v)$  weighting) yielded an essentially symmetric  $\sim 13.75$  arcsec FWHM beam. The 31  $\sim 42.5$  km s<sup>-1</sup> channels were centered on 4541 km s<sup>-1</sup> (channel 16), with channels 11 through 21 containing all of the HI emission. Continuum subtraction was accomplished in  $(u,v)$  space. We will discuss these observations in detail in Sect. 3.2.

### 3.2 The interaction geometry and its consequences

The optical appearance of the NGC 6745 system, and in particular the locations of the numerous bright blue star forming complexes, are suggestive of a tidal passage by the small northern companion galaxy (NGC 6745c; nomenclature from Karachentsev, Karachentseva & Shcherbanovskii 1978) across the eastern edge of the main galaxy, NGC 6745a. The high relative velocities of the two colliding galaxies likely caused ram pressures at the surface of contact between the interacting interstellar clouds in both galaxies, which – in turn – are responsible for the triggering of enhanced star formation, most notably in the interaction zone in between the two galaxies, NGC 6745b.

We analysed our VLA HI observations with as principal aim to assess whether we could confirm this scenario, at least qualitatively, and if we could, therefore, derive the interaction time-scale from our cluster analysis. The interaction-induced cluster formation scenario is at least qualitatively supported by the HI zeroth-moment map of the system,

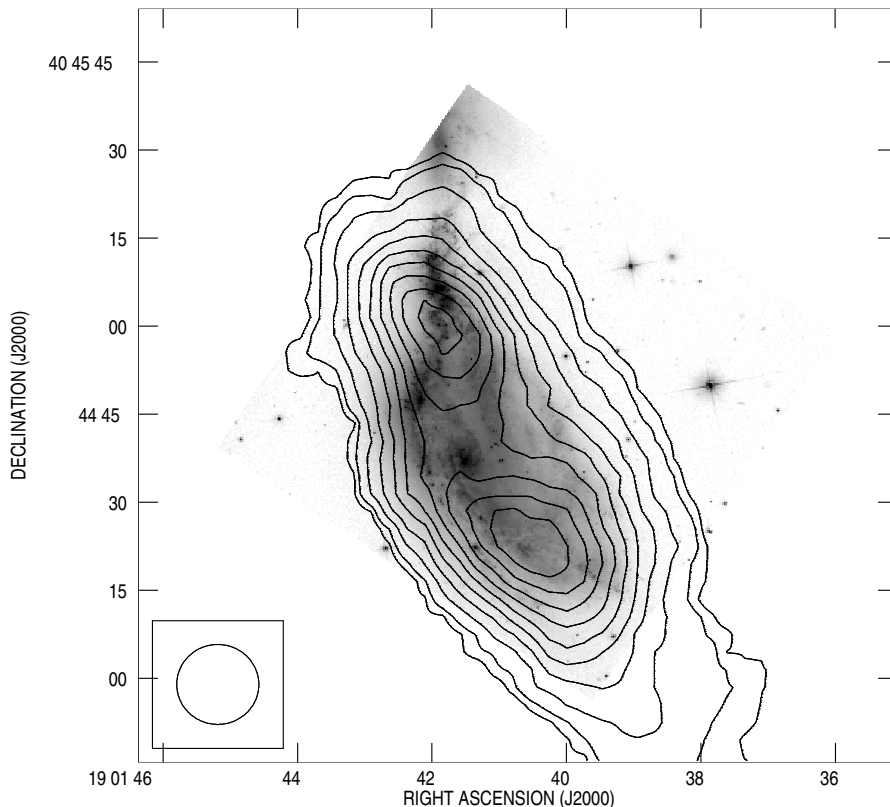


**Figure 7.** NGC 6745 HI distribution shown as contours superimposed on a negative logarithmic reproduction of the F555W *HST*/WFPC2 image of the galaxy. The VLA/C beam size is 13.75 arcsec (FWHM) and is indicated in the lower left corner. Contour intervals are 10 per cent of the maximum flux density of the southern maximum,  $9.565 \times 10^2 \text{ Jy beam}^{-1} \text{ m s}^{-1}$ , except for the lowest contour, which is at 5 per cent of the maximum. Note the East-West asymmetry, the stretching of the lowest contours to the South, and the absence of detectable emission from the northern galaxy. For reference, the (J2000) centre coordinates of NGC 6745a and c are R.A. =  $19^{\text{h}}01^{\text{m}}41.8^{\text{s}}$ , Dec =  $40^{\circ}44'40''$  and R.A. =  $19^{\text{h}}01^{\text{m}}42.0^{\text{s}}$ , Dec =  $40^{\circ}45'35''$ , respectively.

shown overlaid on the optical *WFPC2* image in Fig. 7, and the HI velocity (first moment) map of Fig. 8. First, we point out that there is no evidence for HI emission from the northern galaxy. This is consistent with the absence of significant recent star formation observed in this component (but see Sect. 3.3.2).

The slight distortions in the symmetry of the overall HI distribution along and perpendicular to the direction of elongation may, in fact, be consistent with tidal effects by a small, low-mass intruder (i.e., NGC 6745c). At the northern end of the HI distribution the relevant time-scales are likely so short that we would not expect to see any significant amounts of tidally stretched HI gas, which seems to be the case. At the southern end of the system, on the other hand, where the time elapsed since the alleged South-to-North passage of the intruder is much longer, we see the expected (asymmetric) extension of the lower contours of the HI distribution, as well as a high velocity of approach at the very bottom of our field of view, which may be qualitatively consistent with a trajectory of approach for the intruder. This interpretation is quantitatively supported by CO(1–0) line observations of this system by Zhu et al. (1999), who find a similar velocity gradient between the southern component and the centre of the main galaxy.

The velocity data (Fig. 8) were fit with a Brandt func-

tion (Brandt 1960, Brandt & Belton 1962), weighting the velocities with the square of the intensity data (Fig. 7). The residual map showed excellent agreement over all but the lowest-intensity regions. The best-fitting parameters include (i) systemic velocity,  $v_{r,\odot} = 4528 \text{ km s}^{-1}$  at 4 arcsec West and 2 arcsec South of the optical nucleus; (ii) position angle of the line of nodes = 36 degrees; (iii) inclination of the fundamental plane of the galaxy  $i = 47$  degrees; and (iv) half-amplitude value =  $185 \text{ km s}^{-1}$  reached at  $\sim 32$  arcsec from the location of the kinematic centre. The sense of the rotation of the HI means that the perturbing galaxy, NGC 6745c, is in a prograde orbit, which favours a strong and rapid gravity-wave response in the affected galaxy, NGC 6745a.

VLA continuum observations at 1.425 GHz (Condon et al. 1996) show a more compact morphology, which more closely follows the system's stellar distribution and far-infrared appearance (IRAS; e.g., Bushouse et al. 1988, Condon et al. 1995, Sanders et al. 1995). As opposed to our  $\sim 1.4$  GHz line observations that predominantly trace the cold HI component, the continuum flux has a non-thermal origin, as evidenced by the 1.4–5 GHz spectral index of between +0.75 and +0.83 (Condon et al. 1991, 1995).

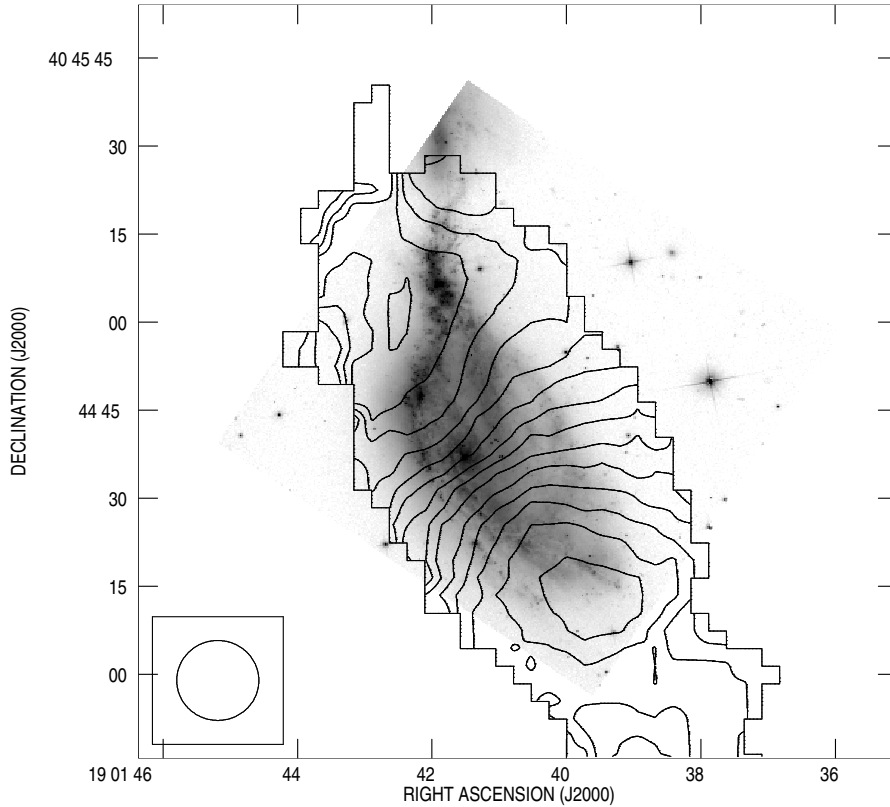


**Figure 8.** NGC 6745 HI radial velocity distribution shown as contours superimposed on a negative logarithmic reproduction of the F555W *HST*/WFPC2 image of the galaxy. The VLA/C beam size is 13.75 arcsec (FWHM) and is indicated in the lower left corner. Contours are at intervals of 20 km s<sup>-1</sup> beginning at 4400 km s<sup>-1</sup> for the smallest entire contour South West of the center enclosing the minimum of 4388 km s<sup>-1</sup> and ending with the smallest entire contour North East of the center enclosing the maximum of 4661 km s<sup>-1</sup>. The “boxy” outer line encloses map data  $> 8.14 \times 10^{-4}$  Jy beam<sup>-1</sup> ( $3 \sigma$ ) used in the moment calculations. The contours exhibit, in general, the splayed structure that is characteristic of rotating disks common in late-type spiral galaxies.

### 3.3 Properties of the star-forming regions

Since the morphology and appearance of the NGC 6745 system are consistent with the scenario favouring a very recent tidal encounter and its associated triggered star and star cluster formation, we will now use the main properties of the star clusters and star forming complexes, such as their ages, masses and metallicities, to derive boundary conditions for the physical conditions governing such minor merger events.

With the lessons learnt from Paper I in mind, we applied a similar three-dimensional  $\chi^2$  minimisation (with respect to the Anders & Fritze-v. Alvensleben [2003] models) to the spectral energy distributions (SEDs) of our star cluster candidates and star forming complexes to obtain the most likely combination of age, mass, metallicity  $Z$  and internal extinction  $E(B - V)$  (assuming a Calzetti et al. [2000] starburst galaxy-type extinction law for the internal extinction) for each individual object. Galactic foreground extinction towards NGC 6745 was taken from Schlegel et al. (1998). The resulting age, mass, metallicity and extinction distributions for the NGC 6745 objects are shown in Fig. 9.

#### 3.3.1 Effects of the age–metallicity degeneracy

Based on the knowledge gained in Paper I, we suspected that the strong peak at young ages ( $\log(\text{Age}/\text{yr}) \sim 6.8$ ; see

Fig. 9a) might be an artefact caused by the age–metallicity degeneracy. Therefore, we display these particular clusters as the shaded histograms in Figs. 9b, c and d. It is clear from an examination of the NGC 6745 cluster metallicity distribution in Fig. 9c, that the clusters in the young-age peak indeed compose a higher-than-average metallicity peak, thus highlighting the caution required to avoid confusion arising from this degeneracy. As a consequence of the underestimated ages for the clusters affected by the age–metallicity degeneracy, their masses are also biased towards lower-than-average masses. If we now turn this argument around, and examine the properties of the clusters in the second metallicity peak at  $0.015 \lesssim Z \lesssim 0.020$ , we find that those clusters do indeed dominate the young-age peak (as expected; not shown), and are generally biased towards younger ages overall. This confirms the importance of the age–metallicity degeneracy for the broad-band filters used in this paper, and for the young ages of the star clusters and star-forming complexes in NGC 6745. The mass and extinction properties of the clusters in this secondary metallicity peak are consistent with those of the full cluster sample.

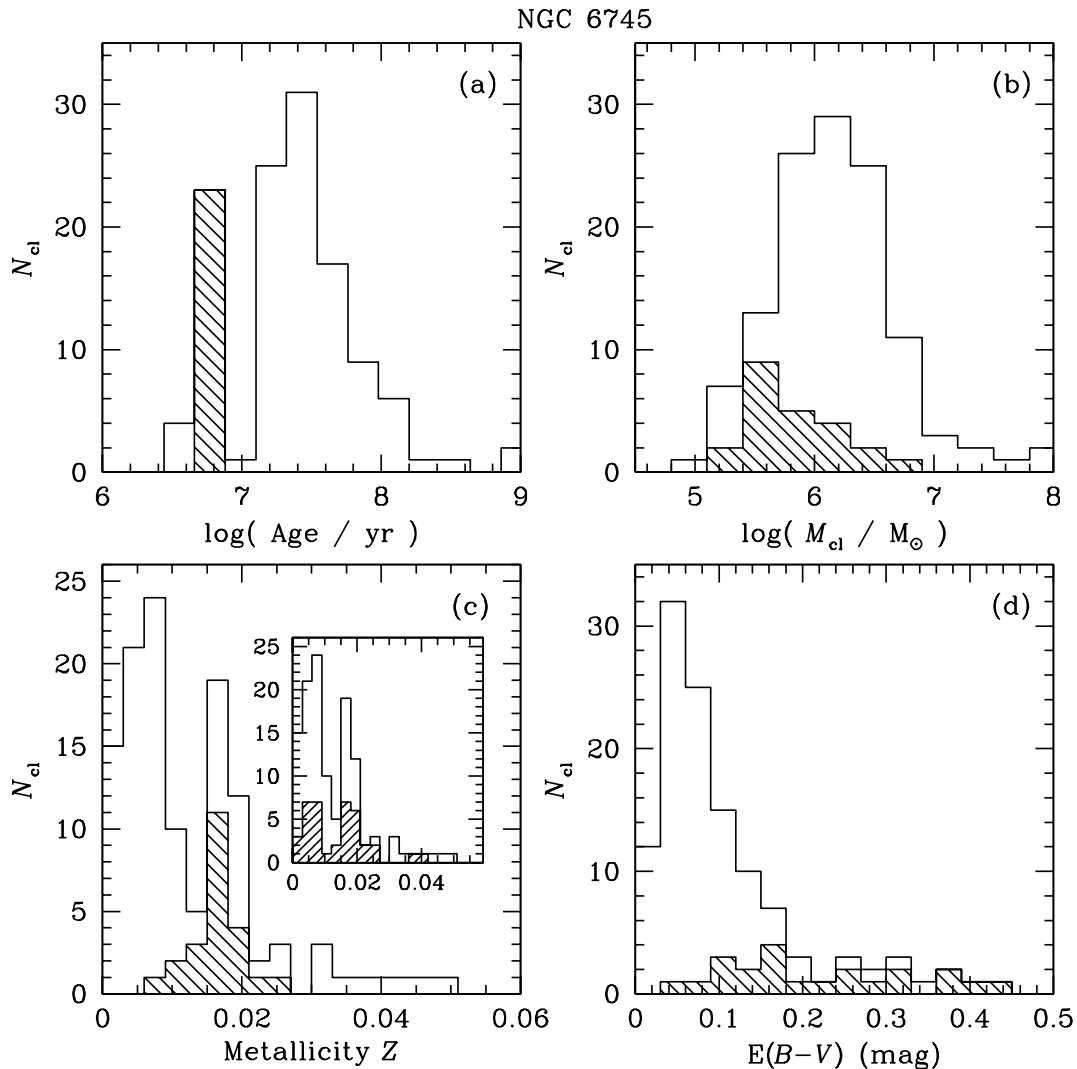


**Figure 9.** Age, mass, metallicity and extinction distributions of the clusters in NGC 6745, based on our 4-passband fitting technique used to determine age, metallicity and extinction estimates simultaneously. Although the main properties of these distributions are reasonably correct, the shaded histograms are affected significantly by the age–metallicity degeneracy: the shaded histograms, corresponding to the young-age peak in panel (a), show a distinct second peak at close-to-solar metallicity (panel c), compared to the other clusters that peak at much lower metallicities. The shaded histogram in the inset in panel (c) is the metallicity distribution of the clusters in the most actively star forming region connecting the main galaxy with its smaller companion.

### 3.3.2 Case for a fixed mean metallicity

In the inset of Fig. 9c we show the metallicity distribution of the entire cluster sample once again, with the clusters from the interaction zone in between the two galaxies highlighted as the inner, shaded histogram. This shaded histogram is characterized by two clear peaks in metallicity. However, if these clusters were all formed approximately coevally (as implied by their derived ages) and in a tightly confined spatial area, their metallicities *must* be very similar; a clearly double-peaked distribution is therefore physically unrealistic and therefore most likely another artefact caused by the age–metallicity degeneracy.

Based on these arguments, it is most likely that the NGC 6745 young cluster system is best approximated by a metallicity consistent with that of the low-metallicity peak in Fig. 9c, at  $Z \lesssim 0.015$ . Therefore, we reapplied our SED

fitting routines to the observational data, assuming a more appropriate fixed metallicity of  $Z = 0.008$  for all clusters. The resulting age and mass distributions, are shown in Figs. 10b and c. We also show (in Fig. 10a) the clusters’ locations in the (age vs. mass) plane with respect to our  $\sim 90\%$  completeness limit at  $m_{F555W} \simeq 23.5$  mag (imposed by the shallow depth of the F336W observations; cf. Fig. 6). The new distribution of extinction estimates, based on the  $Z = 0.008$  assumption, does not differ significantly from that of Fig. 9d.

[We note that, while this procedure likely results in the most realistic cluster parameters for the NGC 6745 system (due to the availability of only four optical passbands), the situation for NGC 3310 is different. Because of the availability of observations of the NGC 3310 cluster system covering a larger number of passbands and a greater wavelength

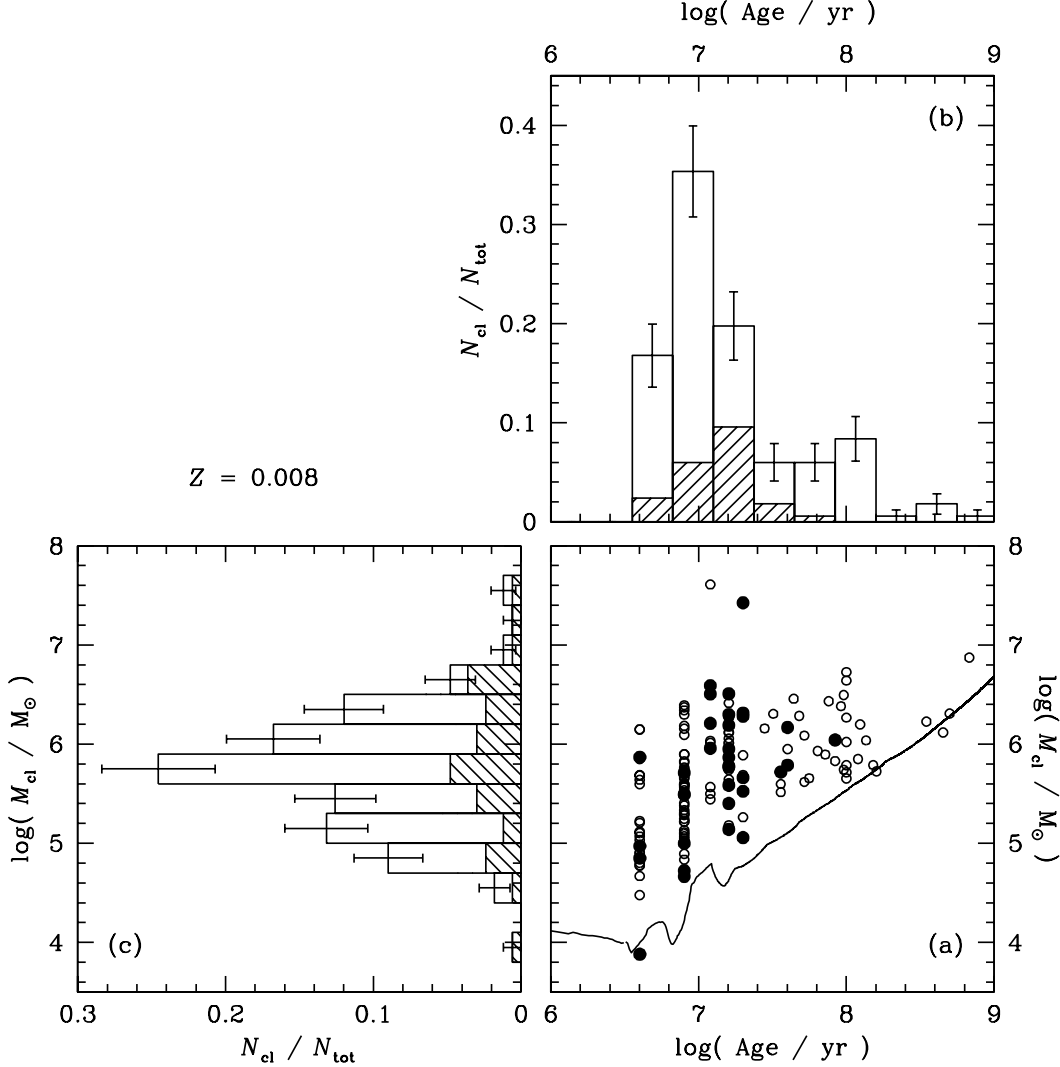


**Figure 10.** (a) – Distribution of the NGC 6745 clusters in the (age vs. mass) plane, assuming a fixed metallicity of  $Z = 0.008$  for all clusters. The solid bullets represent the clusters in the most actively star forming region, i.e. NGC 6745b. Overplotted is the expected, age-dependent detection limit, predicted by the Anders & Fritze-v. Alvensleben (2003) models for the appropriate stellar IMF. This model prediction is based on a detection limit of  $m_{F336W} = 23.5$  and  $(m - M)_{\text{NGC6745}} = 34.17$ , assuming no extinction. (b) and (c) – Distributions of, respectively, the ages and masses of the compact clusters in NGC 6745. The shaded histograms show the distributions of the clusters in NGC 6745b. The uncertainties are of the order of the histogram bin sizes.

range, we concluded that fitting all of our free parameters simultaneously resulted in the best parameter estimates.]

There is an enhancement of cluster formation around  $\log(\text{Age}/\text{yr}) \simeq 7$ , which is therefore our best estimate of the interaction time-scale. The clusters younger than  $\log(\text{Age}/\text{yr}) \simeq 7.4$  ( $\sim 25$  Myr) are all located in either the interaction zone NGC 6745b (see the shaded histogram in Fig. 10b), or among the sprinkling of blue objects resembling a spiral arm on the eastern edge of the main galactic disc. This is consistent with tidally-triggered star (cluster) formation along the proposed trajectory of the companion galaxy across the main disc component of NGC 6745 (see Sect. 3.2). The lower age cut-off at  $\log(\text{Age}/\text{yr}) = 6.6$  (4 Myr) is artificial, and corresponds to the youngest ages included in our SSP models (Schulz et al. 2002, Anders & Fritze-v. Alvensleben 2003); a fraction of our NGC 6745 cluster sample

may therefore have even younger ages. Thus, it seems likely that the interaction began to have a significant effect on the star (cluster) formation history some 25 Myr ago, and has been ongoing until the present.

We detected three compact clusters that are clearly associated with the companion galaxy itself; they are unlikely to originate from the interaction-induced starburst region, NGC 6745b, based on their large projected distances from the interaction zone. Two of these have ages of  $\sim 100$  and  $\sim 140$  Myr, and are located in the general field of its disc. The third, located near the centre of the companion galaxy, is of similar age as the starburst in NGC 6745a and b,  $\sim 8$  Myr. Close inspection of the overall colour distribution of the field star population in NGC 6745c reveals a bluer centre, which might therefore imply that the tidal interaction with the main NGC 6745 galaxy has also induced enhanced

star formation in the companion galaxy, but at a much lower level due to the absence of significant amounts of gas (see Sect. 3.2). The little available gas in NGC 6745c might not have been sufficient for the formation of star *clusters*.

There is no clear spatial dependence of the cluster masses, although the lowest-mass clusters appear to originate in the lowest-density regions. This is most likely an observational selection effect, however. Although the galaxy's distance, combined with the photometric depth of the observations, prevents us from probing below  $\log(M_{\text{cl}}/M_{\odot}) = 5.0$  for clusters older than  $\sim 10$  Myr, we point out that there is a significant population of high-mass clusters or cluster complexes, with masses in the range  $6.5 \lesssim \log(M_{\text{cl}}/M_{\odot}) \lesssim 8.0$ . We have checked the reality and signal-to-noise ratio of the SED of each of these objects individually, and have only retained those objects that appear real beyond any reasonable doubt. These clusters do not have counterparts among the Galactic GCs (e.g., Mandushev, Staneva & Spassova 1991, Pryor & Meylan 1993). In fact, these masses are similar to or exceed the spectroscopically confirmed mass estimates of the so-called “super star clusters” (SSCs) in M82 (M82-F; Smith & Gallagher 2001), and the Antennae galaxies (Mengel et al. 2002). Our detection of similarly massive SSCs in NGC 6745, which are mostly located in the intense interaction zone, NGC 6745b, supports the scenario that such objects form preferentially in the extreme environments of interacting galaxies.

We caution, however, that these massive SSC candidates may not be gravitationally bound objects, but more diffuse star forming regions or aggregates of multiple unresolved clusters instead. Even with the unprecedented *HST* spatial resolution, we cannot distinguish between these possibilities. Nevertheless, we measure an effective radius for the most massive object ( $M_{\text{cl}} \simeq 5.9 \times 10^8 M_{\odot}$ ) of only  $R_{\text{eff}} \sim 16$  pc. However, this object appears very elongated, or may in fact be a double cluster. We should keep in mind, of course, that this high mass estimate is a strong function of the (low) metallicity assumed; if we had assumed solar metallicity for this object, the derived age would have been significantly smaller ( $\sim 10 - 20$  Myr vs.  $\sim 1$  Gyr), and the mass could be smaller by a factor of  $\gtrsim 10$ . Even so, if we could confirm this mass estimate spectroscopically, either of the subcomponents would be the most massive cluster known to date, significantly exceeding cluster W3 in NGC 7252, which has a mass of about  $(3-18) \times 10^7 M_{\odot}$ , depending on the age, metallicity and IMF assumed (Schweizer & Seitzer 1998, Maraston et al. 2001).

### 3.4 The initial cluster mass distribution

As for NGC 3310, in Figs. 11a and b we show the NGC 6745 cluster formation rate (per linear time period) and its mass spectrum, respectively. For our analysis of the cluster disruption time-scales in NGC 6745 we will make the same assumptions as described in Sect. 2.2. The long-dashed line in Fig. 11a for the youngest ages,  $\log(\text{Age}/\text{yr}) \leq 8$ , is the expected effect of a fading SSP in the F336W filter (which determines our sample completeness for this galaxy), for a constant on-going cluster formation rate, shifted vertically to best match the data points for  $\log(\text{Age}/\text{yr}) \leq 7.25$ , and limited by the completeness in the F336W observations. For this band, the predicted fading line is horizontal at  $\log(\text{Age}/\text{yr}) \lesssim 6.5$  and

has a slope of  $-1.12$  for older clusters, in the parameter space of Fig. 11a. The short-dashed lines in both Figs. 11a and b are the best-fitting power-law slopes, obtained for the age and mass ranges  $\log(\text{Age}/\text{yr}) \geq 7.4$  and  $\log(M_{\text{cl}}/M_{\odot}) \geq 5.6$ , while the dotted lines indicate the likely uncertainties in the slopes. The latter were obtained from subsets of the data points used for the dashed fits, which were determined over the full ranges. The vertical dashed and dotted lines in Fig. 11b at  $\log(M_{\text{cl}}/M_{\odot}) = 4.75$  and  $\log(M_{\text{cl}}/M_{\odot}) = 5.4$  correspond to our formal completeness limit, for a peak young cluster age of  $\log(\text{Age}/\text{yr}) = 7.0$  and for the significant fraction of sample clusters with ages up to  $\log(\text{Age}/\text{yr}) = 8.0$ , respectively. Thus, it follows that incompleteness plays at least some role for masses up to  $\log(M_{\text{cl}}/M_{\odot}) \sim 5.4$ .

For  $\log(\text{Age}/\text{yr}) \geq 7.25$  we find a best-fitting slope of  $(1 - \alpha)/\gamma = -1.86(\pm 0.20)_{-0.06}^{+0.21}$ , where the first uncertainty represents the formal uncertainty in the fit and the second the likely uncertainty resulting from our choice of fitting range (i.e., the dotted fits in Fig. 11a). Assuming that  $\alpha = 2.0$  (see below) we find that  $\gamma = 0.54 \pm 0.06$ , close to the mean value of 0.62 derived by BL03 for cluster samples in four galaxies.

The crossing point of the two power laws of the age distribution is at  $\log(t_{\text{cross}}/\text{yr}) \simeq 7.3$ . Substituting these values into Eq. (15) of BL03, we obtain a characteristic disruption time-scale for  $10^4 M_{\odot}$  clusters of  $\log(t_4^{\text{dis}}/\text{yr}) = 7.75$ . This implies that the disruption time-scale of clusters more massive than  $\sim 4 \times 10^5 M_{\odot}$  is longer than  $5.5 \times 10^8$  yr. All clusters in our sample, with one exception, are younger than this. The mass distribution of clusters more massive than  $4 \times 10^5 M_{\odot}$ , shown in Fig. 11a, has a slope of  $-1.96(\pm 0.15) \pm 0.19$ , where the first uncertainty again represents the formal uncertainty in the fit and the second the likely uncertainty resulting from our choice of fitting range (i.e., the dotted fits in Fig. 11b). Since these massive clusters have not yet suffered disruption, the measured slope represents that of the cluster IMF of NGC 6745.

## 4 THE INITIAL CLUSTER MASS FUNCTION

For star cluster systems as young as the tidally-induced cluster populations in NGC 3310 and NGC 6745, for which the age of the starburst in which they were formed is significantly smaller than their respective characteristic cluster disruption time-scales, we have shown that the application of the empirical cluster disruption models of BL03 results in an independent estimate of the *initial* cluster mass function slope,  $\alpha$ . For the NGC 3310 and NGC 6745 cluster systems,  $\alpha = 2.04(\pm 0.23)_{-0.43}^{+0.13}$  and  $1.96(\pm 0.15) \pm 0.19$ , respectively, for masses  $M_{\text{cl}} \gtrsim 10^9 M_{\odot}$  and  $M_{\text{cl}} \gtrsim 4 \times 10^5 M_{\odot}$ .

The slopes of the CLFs of young star cluster systems, and to some lesser extent those of their mass functions as well, have been studied extensively – in particular since the launch of the *HST* – in a wide variety of star-forming environments, including interacting and starburst galaxies, circumnuclear starburst rings, and also in “normal” spiral and irregular galaxies by means of the HII region luminosity function (regarding the latter, see e.g. Kennicutt & Hodge 1980, Kennicutt et al. 1989, Arsenault et al. 1990, Cepa & Beckman 1990, Caldwell et al. 1991, Banfi et al. 1993, Elmegreen & Salzer 1999; and simulations by Oey & Clarke 1998). In

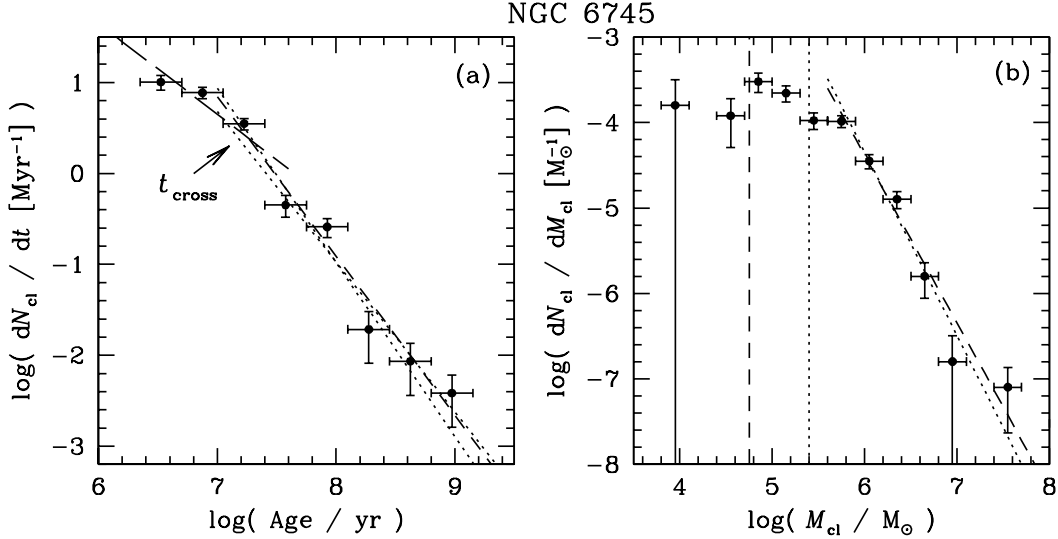


**Figure 11.** (a) – The cluster formation rate (in number of clusters per Myr) in NGC 6745 as a function of age. The long-dashed line for  $\log(\text{Age}/\text{yr}) \leq 8.0$  is the expected effect of a fading SSP, for a constant ongoing cluster formation rate, shifted vertically to best match the data points for  $\log(\text{Age}/\text{yr}) \leq 7.25$ , and limited by the completeness of our F336W observations. The short-dashed and dotted lines are our best fit for greater ages and the maximum likely deviation from this best fit, respectively. (b) – Mass spectrum of the NGC 6745 clusters (number of clusters per mass bin); line encoding as in panel (a). The vertical dashed line at  $\log(M_{\text{cl}}/M_{\odot}) = 4.75$  corresponds to our 90% completeness limit for a cluster age of  $\log(\text{Age}/\text{yr}) = 7.0$ . The vertical dotted line corresponds to the same completeness limit, but for a cluster age of  $\log(\text{Age}/\text{yr}) = 8.0$ .

Table 2, we give an overview of the CLF (and, in a few cases, of the mass function) slopes based on determinations available in the literature, both for young cluster systems in interacting and starburst galaxies, and for cluster populations in circumnuclear starburst rings.

In addition to these galaxies, Meurer et al. (1995) found that the CLF slope of the combined sample of SSCs in 9 starburst galaxies, for  $M_{\text{F220W}} \lesssim -14$ , is consistent with  $\alpha = 2$ ; Maoz et al. (1996) constructed the combined CLF for the circumnuclear ring clusters in NGC 1433, NGC 1512 and NGC 2997, based on UV observations, and reached a similar conclusion for the high-luminosity end of their CLF. Finally, Crocker et al. (1996) analysed the HII region luminosity function in 32 (pseudo-)ringed S0 – Sc galaxies, and found a mean  $\langle \alpha \rangle = 1.95 \pm 0.25$ .

Thus, in all but a few cases (e.g., M82 B), the CLF and, where derived, the mass function slopes of the young clusters are similar ( $\alpha \simeq 2$ ) among a wide variety of galaxies, including those in which the star and cluster formation process is dominated by strong tidal forces, and systems of a more quiescent nature (e.g., normal spiral and irregular galaxies; Kennicutt et al. 1989, Banfi et al. 1993, Elmegreen & Salzer 1999). One should keep in mind that the observed CLF is the result of both the original mass distribution of the young star clusters and the giant molecular clouds (GMCs) they originated from, and subsequent cluster disruption processes (e.g., Harris & Pudritz 1994, Bik et al. 2003, BL03, de Grijs et al. 2003b); in de Grijs et al. (2003b) and Parmentier et al. (2003) we showed that the M82 B cluster system must have undergone significant disruption owing to the unusually short characteristic cluster disruption time-scale,  $\log(t_{\text{dis}}/\text{yr}) \simeq 7.5 + 0.62 \times \log(M_{\text{cl}}/10^4 M_{\odot})$  (de Grijs

et al. 2003b), so that the observed shallow(er) CLF and mass function slopes do not represent the *initial* cluster mass function slope anymore. However, in most other young cluster systems known the expected characteristic cluster disruption time-scales are well in excess of the median age of the cluster system, so that at least the high-luminosity (high-mass) end of the CLF (and cluster mass function) remains likely unaffected by significant alterations caused by disruption (e.g., Buta et al. 1999, Zhang & Fall 1999, Bik et al. 2003, Paper I). In this paper, we have derived very similar *mass* function slopes, and have also properly accounted for the effects of cluster disruption.

Under the usual assumption that the stellar mass-to-light ratio does not vary significantly over the age range of a given young cluster system, or – alternatively – after correcting the observed CLF to a common age (e.g., Meurer 1995, Fritze-v. Alvensleben 1999, de Grijs et al. 2001, 2003a,b), the resulting CLF slope can be interpreted in terms of the intrinsic cluster mass distribution. The observed mass function slope,  $\alpha \simeq 2$ , is very similar to those of the mass functions of Galactic open star clusters (e.g., van den Bergh & Lafontaine 1984, Elson & Fall 1985), GMCs (e.g., Casoli, Combes & Gerin 1984, Sanders, Scoville & Solomon 1985, Solomon et al. 1987, Solomon & Rivolo 1989, Williams & McKee 1997) and GMC cores (e.g., Harris & Pudritz 1994, Williams, de Geus & Blitz 1994, McLaughlin & Pudritz 1996 and references therein; see also the review by Blitz 1991), and to that of the young compact cluster system in the Large Magellanic Cloud (LMC; e.g., Elson & Fall 1985, Elmegreen & Efremov 1997). Thus, it appears that the formation of young compact star clusters, such as the ones discussed in the current series of papers, and of open clusters, GMCs and stellar OB asso-

**Table 2.** Cluster luminosity and mass function slopes based on previous determinations in the literature

Galaxy	Slope ( $-\alpha$ )	Notes	Reference
A. Interacting and Starburst Galaxies			
NGC 1275	$\sim -2$	$M_V < -12$	Holtzman et al. (1992)
	$\sim -2$	$M_B < -8$	Carlson et al. (1998)
NGC 1316	$-1.7 \pm 0.1$	3 Gyr-old merger remnant	Goudfrooij et al. (2001)
NGC 3256	$\sim -1.8$	$M_B \lesssim -9.5$ ; $M_I \lesssim -10.5$	Whitmore et al. (2002)
NGC 3610	$-1.78 \pm 0.05$	$V < 26$ ; red, metal-rich clusters	Zepf et al. (1999)
	$-1.90 \pm 0.07$	corrected for observational scatter	Whitmore et al. (2002)
NGC 3921	$-2.1 \pm 0.3$	$M_V \leq 8.5$	Schweizer et al. (1996)
	$-2.01 \pm 0.22$	corrected for contamination by old GCs	
NGC 4038/39	$-1.78 \pm 0.05$	$-15.5 \leq M_V \leq -10$ ; no completeness corrections	Whitmore & Schweizer (1995)
	$-2.12 \pm 0.04$	$-14 < M_V < -8$ , but contaminated by stars	Whitmore et al. (1999)
	$-2.6 \pm 0.2$	$-14 \leq M_V \leq -10.4$ , corrected for contamination by stars	
	$-1.7 \pm 0.2$	$-10.4 \leq M_V \leq -8$ , corrected for contamination by stars	
	$-1.95 \pm 0.03$	$6.4 < \log(\text{Age/yr}) < 6.8$ ; $10^4 \leq M_{\text{cl}} \leq 10^6 M_\odot$	Zhang & Fall (1999)
	$-2.00 \pm 0.08$	$7.4 < \log(\text{Age/yr}) < 8.2$ ; $10^4 \leq M_{\text{cl}} \leq 10^6 M_\odot$	
NGC 7252	$\sim -2$	$M_V \leq -12$	Whitmore et al. (1993)
	$-1.90 \pm 0.04$	$M_V \leq -8$ , inner sample	Miller et al. (1997)
	$-1.80 \pm 0.07$	$M_V \leq -8$ , outer sample	
M51	$-2.1 \pm 0.3$	$2.5 \times 10^3 < M_{\text{cl}} < 5 \times 10^4 M_\odot$ ; $\log(\text{Age/yr}) < 7$	Bik et al. (2003)
	$-2.0 \pm 0.05$	$2.5 \times 10^3 < M_{\text{cl}} < 2 \times 10^4 M_\odot$ ; $\log(\text{Age/yr}) < 7$	
M82 B	$-1.2 \pm 0.3$	$M_V \lesssim -11$	de Grijs et al. (2001)
	$-1.4 \pm 0.2$	$8.6 < \log(\text{Age/yr}) < 9.1$	Parmentier et al. (2003)
B. Circumnuclear Starburst Rings			
NGC 1097	$\sim -2$	$-14 \lesssim M_V \lesssim -11$	Barth et al. (1995)
NGC 1512	$\sim -2$	$10^3 \lesssim M_{\text{cl}} \lesssim 10^5 M_\odot$	Maoz et al. (2001)
NGC 2997	$\sim -2$		Maoz et al. (1996)
	$-1.97 \pm 0.03$	$M_V \leq -9$	Elmegreen et al. (1999)
NGC 3310	$-2.2 \pm 0.03$	$M_B < -10.5$	Elmegreen et al. (2002)
	$-2.4 \pm 0.04$	from <i>HST</i> <i>K</i> -band data	
	$-1.75 \pm 0.03$	large-scale cluster complexes, <i>K</i> band	
	$-1.8 \pm 0.4$	$17.7 \leq m_{\text{F606W}} \leq 20.2$	Paper I
NGC 5248	$\sim -2$	$10^3 \lesssim M_{\text{cl}} \lesssim 10^5 M_\odot$	Maoz et al. (2001)
NGC 6951	$-2.12 \pm 0.04$	$M_V \leq -9$	Elmegreen et al. (1999)
ESO 565-11	$-2.18 \pm 0.06$	$M_V \leq -8.9$ ; Cluster ages 4–6 Myr	Buta et al. (1999)

ciations (e.g., Elmegreen & Efremov 1997, Elmegreen 2002) is driven by similar physical processes, which results naturally from models advocating that the mass distribution of the progenitor GMCs is well approximated by a turbulence-driven fractal structure, allowing cloud growth by agglomeration (e.g., Harris & Pudritz 1994, Elmegreen & Efremov 1997, Elmegreen et al. 1999, Elmegreen 2002).

## 5 SUMMARY AND CONCLUSIONS

Both NGC 3310 and NGC 6745 are examples of nearby interacting galaxies undergoing intense, tidally-triggered starbursts. The production of luminous, compact star clusters seems to be a hallmark of intense star formation. It is likely that a large fraction of the star formation in starbursts takes place in the form of such concentrated clusters. The basic cluster properties, including their sizes, luminosities, and – in several cases – spectroscopic mass estimates are entirely consistent with what is expected for young Galaxy-type GCs. Young compact star clusters are therefore important because of what they can tell us about GC formation and evolution. They are also important as probes of the history of star formation, chemical evolution, IMF, and other physical characteristics in starbursts.

In this paper we have used the basic properties of the rich young star cluster systems in both starburst galaxies, including estimates of the individual cluster ages, masses, metallicities, and extinction values, to derive the cluster for-

mation history and the subsequent evolution of the star cluster systems as modified by the effects of cluster disruption. Cluster disruption processes must be taken into account for the determination of the cluster formation history from the age distribution of a magnitude-limited cluster sample, because the observed age distribution is that of the surviving clusters only.

For the NGC 3310 star cluster system we used the basic properties obtained in Paper I, which were based on the detailed comparison of updated model SSPs (including the contributions of gaseous, nebular emission) with the clusters' SEDs derived from broad-band *HST* imaging observations. We applied our improved understanding of the systematic uncertainties involved in such an exercise (Paper I) to simultaneously determine robust cluster ages, masses, metallicities and extinction values for the tidally-induced young star cluster system in NGC 6745, based on imaging observations in the minimum of four broad-band passbands covering the entire optical wavelength range from the *HST*-equivalent *U* to *I*-band filters. We further expanded our analysis of the systematic uncertainties involved in this type of analysis by examining the effects of *a priori* assumptions of the individual cluster metallicities. We find that – if observations covering a sufficiently large optical/NIR wavelength range are available – (i) it is very important to determine all of the free parameters (age, metallicity, and extinction, and the corresponding mass estimates) *independently* for each individual cluster, instead of assuming a generic value for any of these parameters (such as assuming a fixed metallicity); and (ii)

the widths of the resulting age and mass distributions, under the assumption of a fixed metallicity for all clusters, are broader than their intrinsic widths owing to the propagation of model and measurement uncertainties.

The central morphology of NGC 3310 is dominated by a bright starburst ring containing a large number of young star clusters. The age (and metallicity) distributions of both the clusters in the ring and of the sample of clusters outside the ring are statistically indistinguishable, with a peak in the age distribution at  $\log(\text{Age}/\text{yr}) \simeq 7.45$ , but the ring clusters appear to peak at slightly greater masses than those found outside the ring. The overabundance of low-mass clusters outside the ring compared to their counterparts in the starburst ring might (at least partially) be due to a spatial dependence of the completeness fraction, but there is a clear and significant excess of higher-mass clusters *in* the ring compared to the non-ring cluster sample, even after taking the systematic uncertainties in our mass estimates into account. It appears that the physical conditions in the starburst ring, such as caused by the effects of the proposed bar-driven instabilities, the higher density of the ISM, and the associated higher likelihood to encounter significant propagating shock waves, may be conducive for the formation of higher-mass star clusters, on average, than in the relatively more quiescent environment of the main galactic disc.

We furthermore conclude that the starburst producing the NGC 3310 ring clusters has been ongoing for at least the past 40 Myr, at an approximately constant cluster formation rate during the burst period. Star cluster formation has proceeded at a similar rate in the central disc of the galaxy; due to the extreme youth of both samples of starburst-induced star clusters, statistically significant differences between the age distributions of the ring and non-ring populations have not yet had time to develop, which implies that we are still observing at least part of the cluster sample in the environment determined by their initial conditions.

For the NGC 6745 cluster system we derive a median age of  $\sim 10$  Myr, assuming a fixed metallicity of  $Z = 0.008$  to avoid the significant effects of the age–metallicity degeneracy for these young ages. Based on the age distribution of the star clusters, and the HI morphology of the interacting system as observed with the VLA, we qualitatively confirm the interaction-induced enhanced star formation scenario. NGC 6745 contains a significant population of high-mass clusters, with masses in the range  $6.5 \lesssim \log(M_{\text{cl}}/M_{\odot}) \lesssim 8.0$ . These clusters do not have counterparts among the Galactic GCs, but are similar to or exceed the spectroscopically confirmed mass estimates of the SSCs in M82 and the Antennae galaxies. Our detection of such massive SSCs in NGC 6745, which are mostly located in the intense interaction zone, NGC 6745b, supports the scenario that such objects form preferentially in the extreme environments of interacting galaxies.

For star cluster systems as young as the tidally-induced cluster populations in NGC 3310 and NGC 6745, for which the age of the starburst in which they were formed is significantly lower than their respective characteristic cluster disruption time-scales (of, respectively,  $\log(t_4^{\text{dis}}/\text{yr}) = 8.05$  and 7.75), we have shown that the application of the empirical cluster disruption models of BL03 results in an independent estimate of the *initial* cluster mass function slope,  $\alpha$ . For the NGC 3310 and NGC 6745 cluster systems,

$\alpha = 2.04(\pm 0.23)_{-0.43}^{+0.13}$  and  $1.96(\pm 0.15) \pm 0.19$ , respectively, for masses  $M_{\text{cl}} \gtrsim 10^5 M_{\odot}$  and  $M_{\text{cl}} \gtrsim 4 \times 10^5 M_{\odot}$ . These mass function slopes are consistent with those of other young star cluster systems in interacting and starburst galaxies, circumnuclear starburst rings, and of the HII region luminosity (and mass) functions in “normal” spiral and irregular galaxies. They are also very similar to the mass function slopes of Galactic open clusters and (OB) associations, of GMCs and their cores, and of the young compact clusters in the LMC. It has been shown previously that this can be understood if the mass function of the progenitor GMC is approximated by a turbulence-driven fractal structure, allowing cloud growth by agglomeration.

## ACKNOWLEDGMENTS

This paper is based on archival observations with the NASA/ESA *Hubble Space Telescope*, obtained at the Space Telescope Science Institute (STScI), which is operated by the Association of Universities for Research in Astronomy (AURA), Inc., under NASA contract NAS 5-26555. This paper is also partially based on ASTROVIRTEL research support, a project funded by the European Commission under 5FP Contract HPRI-CT-1999-00081. This research has made use of NASA’s Astrophysics Data System Abstract Service. RdG acknowledges partial support from The British Council under the *UK–Netherlands Partnership Programme in Science*, additional funding from the Particle Physics and Astronomy Research Council (PPARC), and hospitality at the Astronomical Institute of Utrecht University on several visits. PA is partially supported by DFG grant Fr 916/11-1; PA also acknowledges partial funding from the Marie Curie Fellowship programme EARASTARGAL “The Evolution of Stars and Galaxies”, funded by the European Commission under 5FP contract HPMT-CT-2000-00132.

## REFERENCES

- Anders P., Fritze-v. Alvensleben U., 2003, *A&A*, 401, 1063  
 Arsenault R., Roy J.-R., Boulesteix J., 1990, *A&A*, 234, 23  
 Banfi M., Rampazzo R., Chincarini G., Henry R.B.C., 1993, *A&A*, 280, 373  
 Barth A.J., Ho L.C., Filippenko A.V., Sargent W.L.W., 1995, *AJ*, 110, 1009  
 Bik A., Lamers H.J.G.L.M., Bastian N., Panagia N., Romaniello M., 2003, *A&A*, 397, 473  
 Blitz L., 1991, in Lada C.J., Kylafis N.D., eds., *The Physics of Star Formation and Early Stellar Evolution*, NATO ASI Series, Dordrecht: Kluwer, p. 3  
 Bouloukos S.G., Lamers H.J.G.L.M., 2003, *MNRAS*, 338, 717 (BL03)  
 Brandt J.C., 1960, *ApJ*, 131, 293  
 Brandt J.C., Belton M.J.S., 1962, *ApJ*, 136, 352  
 Bushouse H.A., Werner M.W., Lamb S.A., 1988, *ApJ*, 335, 74  
 Buta R., Crocker D.A., Byrd G.G., 1999, *AJ*, 118, 2071  
 Caldwell N., Kennicutt R., Phillips A.C., Schommer R.A., 1991, *ApJ*, 370, 526  
 Calzetti D., Armus L., Bohlin R.C., Kinney A.L., Koornneef J., Storchi-Bergmann T., 2000, *ApJ*, 533, 682  
 Carlson M.N., et al., 1998, *AJ*, 115, 1778  
 Casoli F., Combes F., Gerin M., 1984, *A&A*, 133, 99  
 Cepa J., Beckman J.E., 1990, *A&AS*, 83, 211  
 Chernoff D.F., Weinberg M.D., 1990, *ApJ*, 351, 121

- Condon J.J., Anderson E., Broderick J.J., 1995, *AJ*, 109, 2318  
 Condon J.J., Frayer D.T., Broderick J.J., 1991, *AJ*, 101, 362  
 Condon J.J., Helou G., Sanders D.B., Soifer B.T., 1996, *ApJS*, 103, 81  
 Conselice C.J., Gallagher J.S., Calzetti D., Homeier N., Kinney A.L., 2000, *AJ*, 119, 79  
 Conti P.S., Leitherer C., Vacca W.D., 1996, *ApJ*, 461, L87  
 Crocker D.A., Baugus P.D., Buta R., 1996, *ApJS*, 105, 353  
 de Grijs R., Bastian N., Lamers H.J.G.L.M., 2003a, *ApJ*, 583, L17  
 de Grijs R., Bastian N., Lamers H.J.G.L.M., 2003b, *MNRAS*, 340, 197  
 de Grijs R., Fritze-v. Alvensleben U., Anders P., Gallagher J.S. III, Bastian N., Taylor V.A., Windhorst R.A., 2003c, *MNRAS*, in press (astro-ph/0302286; Paper I)  
 de Grijs R., Lee J.T., Mora Herrera M.C., Fritze-v. Alvensleben U., Anders P., 2003d, *New Astron.*, 8, 155  
 de Grijs R., O'Connell R.W., Gallagher J.S. III, 2001, *AJ*, 121, 768  
 de la Fuente Marcos R., 1997, *A&A*, 322, 764  
 Díaz A.I., Álvarez Álvarez M., Terlevich E., Terlevich R., Sánchez Portal M., Aretxaga I., 2000, *MNRAS*, 311, 120  
 Elmegreen B.G., 2002, *ApJ*, 564, 773  
 Elmegreen B.G., Efremov Y.N., 1997, *ApJ*, 480, 235  
 Elmegreen D.M., Chromey F.R., McGrath E.J., Ostenson J.M., 2002, *AJ*, 123, 1381  
 Elmegreen D.M., Chromey F.R., Sawyer J.E., Reinfeld E.L., 1999, *AJ*, 118, 777  
 Elmegreen D.M., Salzer J.J., 1999, *AJ*, 117, 764  
 Elson R.A.W., Fall S.M., 1985, *PASP*, 97, 692  
 Falco E.E., et al., 1999, *PASP*, 111, 438  
 Fritze-v. Alvensleben U., 1999, *A&A*, 342, L25  
 Goudfrooij P., Mack J., Kissler-Patig M., Meylan G., Minniti D., 2001, *MNRAS*, 322, 643  
 Harris W.E., Pudritz R.E., 1994, *ApJ*, 429, 177  
 Ho L.C., 1997, *Rev. Mex. A&A*, 6, 5  
 Ho L.C., Filippenko A.V., 1996a, *ApJ*, 466, L83  
 Ho L.C., Filippenko A.V., 1996b, *ApJ*, 472, 600  
 Holtzman J.A., et al., 1992, *AJ*, 103, 691  
 Karachentsev I.D., Karachentseva V.E., Shcherbanovskii A.L., 1978, *PAZh*, 4, 483 (English transl. in *Soviet Astr. Lett.*, 4, 261)  
 Kennicutt R.C., Jr., Edgar B.K., Hodge P.W., 1989, *ApJ*, 337, 761  
 Kennicutt R.C., Jr., Hodge P.W., 1980, *ApJ*, 241, 573  
 Mandushev G., Staneva A., Spassova N., 1991, *A&A*, 252, 94  
 Maoz D., Barth A.J., Ho L.C., Sternberg A., Filippenko A.V., 2001, *AJ*, 121, 3048  
 Maoz D., Barth A.J., Sternberg A., Filippenko A.V., Ho L.C., Duccio Macchetto F., Rix H.-W., Schneider D.P., 1996, *AJ*, 111, 2248  
 Maraston C., Kissler-Patig M., Brodie J.P., Barmby P., Huchra J.P., 2001, *A&A*, 370, 176  
 McLaughlin D.E., Pudritz R.E., 1996, *ApJ*, 457, 578  
 Mengel S., Lehnert M.D., Thatte N., Genzel R., 2002, *A&A*, 383, 137  
 Meurer G.R., 1995, *Nat.*, 375, 742  
 Meurer G.R., Heckman T.M., Leitherer C., Kinney A., Robert C., Garnett D.R., 1995, *AJ*, 110, 2665  
 Miller B.W., Whitmore B.C., Schweizer F., Fall S.M., 1997, *AJ*, 114, 2381  
 O'Connell R.W., Gallagher J.S., Hunter D.A., 1994, *ApJ*, 433, 65  
 Oey M.S., Clarke C.J., 1998, *AJ*, 115, 1543  
 Parmentier G., de Grijs R., Gilmore G., 2003, *MNRAS*, in press (astro-ph/0302321)  
 Pastoriza M.G., Dottori H.A., Terlevich E., Terlevich R., Díaz A.I., 1993, *MNRAS*, 260, 177  
 Portegies Zwart S.F., Makino J., McMillan S.L.W., Hut P., 2001, *ApJ*, 546, L101  
 Pryor C., Meylan G., 1993, in Djorgovski S.G., Meylan G., eds., *Structure and Dynamics of Globular Clusters*, Astron. Soc. Pac., San Francisco, p. 357  
 Ratnatunga K.U., Bahcall J.N., 1985, *ApJS*, 59, 63  
 Sanders D.B., Egami E., Lipari S., Mirabel I.F., Soifer B.T., 1995, *AJ*, 110, 1993  
 Sanders D.B., Scoville N.Z., Solomon P.M., 1985, *ApJ*, 289, 373  
 Schlegel D.J., Finkbeiner D.P., Davis M., 1998, *ApJ*, 500, 525  
 Schulz J., Fritze-v. Alvensleben U., Möller C.S., Fricke K.J., 2002, *A&A*, 392, 1  
 Schweizer F., Miller B.W., Whitmore B.C., Fall S.M., 1996, *AJ*, 112, 1839  
 Schweizer F., Seitzer P., 1998, *AJ*, 116, 2206  
 Smith D.A., et al., 1996, *ApJ*, 473, L21  
 Smith L.J., Gallagher J.S. III, 2001, *MNRAS*, 326, 1027  
 Solomon P.M., Rivolo A.R., 1989, *ApJ*, 339, 919  
 Solomon P.M., Rivolo A.R., Barrett J., Yahill A., 1987, *ApJ*, 319, 730  
 Spitzer L. Jr., 1957, *ApJ*, 127, 17  
 Telesco C.M., Gatley I., 1984, *ApJ*, 284, 557  
 Twarog B.A., Ashman K.M., Anthony-Twarog B.A., 1997, *AJ*, 114, 2556  
 van den Bergh S., 1995, *Nat.*, 374, 215  
 van den Bergh S., Lafontaine A., 1984, *AJ*, 89, 1822  
 van der Kruit P.C., de Bruyn A.G., 1976, *A&A*, 48, 373  
 Watson A.M., et al., 1996, *AJ*, 112, 534  
 Whitmore B.C., Schweizer F., 1995, *AJ*, 109, 960  
 Whitmore B.C., Schweizer F., Kundu A., Miller B.W., 2002, *AJ*, 124, 147  
 Whitmore B.C., Schweizer F., Leitherer C., Borne K., Robert C., 1993, *AJ*, 106, 1354  
 Whitmore B.C., Zhang Q., Leitherer C., Fall S.M., Whitmore B.C., Miller B.W., 1999, *AJ*, 118, 1551  
 Williams J.P., de Geus E.J., Blitz L., 1994, *ApJ*, 428, 693  
 Williams J.P., McKee C.F., 1997, *ApJ*, 476, 166  
 Zepf S.E., Ashman K.M., English J., Freeman K.C., Sharples R.M., 1999, *AJ*, 118, 752  
 Zhang Q., Fall S.M., 1999, *ApJ*, 527, L81  
 Zhu M., Seaquist E.R., Davoust E., Frayer D.T., Bushouse H.A., 1999, *AJ*, 118, 145